Nuclear Magnetic Resonance Studies of Biopolymer Dynamics

ARTICLE *in* THE JOURNAL OF PHYSICAL CHEMISTRY · JULY 1996

Impact Factor: 2.78 · DOI: 10.1021/jp9606117

3 AUTHORS, INCLUDING:

Ann Mcdermott
Columbia University
100 PUBLICATIONS **3,997** CITATIONS

SEE PROFILE

Nuclear Magnetic Resonance Studies of Biopolymer Dynamics

Arthur G. Palmer III,[‡] John Williams,[†,§] and Ann McDermott*[,†]

Department of Chemistry and Department of Biochemistry and Molecular Biophysics, Columbia University, New York, New York 10027

Received: February 28, 1996; In Final Form: May 8, 1996[⊗]

NMR spectroscopy is a powerful approach for quantitating molecular conformational dynamics at multiple atomic sites and over multiple time scales. Extensive studies by solution and solid-state NMR spectroscopy of spin relaxation and line shapes in biological macromolecules have been performed in order to characterize the amplitudes, time scales, and energetics of intramolecular conformational modes and to elucidate the relationships between conformational dynamics, structure, and function. This review describes NMR spectroscopic methods for investigation of conformational dynamics together with theoretical descriptions appropriate for interpretation and simulation of the techniques, surveys the range of results available from solution and solid state NMR studies of proteins and other biomolecules, and identifies opportunities for further individual and collaborative development of solution and solid state NMR techniques for characterizing the dynamical properties of biological macromolecules.

Introduction

Since the original reports of the detection of nuclear magnetic resonance (NMR) more than 50 years ago, NMR spectroscopy has generated an enormous body of information on molecular conformational dynamics. These data encompass gas, liquid, and solid phase systems and include small molecules as well as macromolecules and polymers. In the area of biopolymers in particular, a recent efflorescence has resulted in numerous solution NMR studies of protein dynamics,[1−3] solid state NMR (SSNMR) studies of amino acid side chain dynamics,[4−6] and a variety of studies of site-specific dynamics in nucleic acids[7] and lipids.[8] A central aim of these investigations is a description of thermally active conformational modes that encapsulates their amplitudes, energetics, and time scales, manifests their dependence on interactions with ligands and other biopolymers, and delineates their relationship to structure and function. Although the pervasiveness and importance of biopolymer motions have been amply documented, analyzing the energetics and modeling the amplitudes and time scales of these motions pose very challenging problems. Connections between molecular dynamics and function remain to be clarified, and the continuing need for experimental data under functionally relevant, near physiological conditions is emphasized.

A consistent nomenclature and conceptual framework is also needed to describe the dynamic properties of proteins and other biological macromolecules. The conformational dynamics of small molecules often can be described by models that incorporate separable degrees of freedom, in which each motional mode is described by an exponentially decaying correlation function. In fact, many processes for simple molecules on the microsecond time scale and slower are associated with correlation times that vary with temperature as predicted by the Arrhenius equation; consequently, activation enthalpies and entropies are useful concepts in describing the kinetics and in comparing experimental and computational results. This paradigm generally has not been successful in describing synthetic polymeric systems: although theoretical interpretations of the dynamic behavior of polymers are under dispute, the experimental kinetics unambiguously are not well described by exponential functions or activated kinetics. Instead, broad distributions of correlation times and effective activation free energies must be invoked to fit the data. Kinetic behaviors of polymeric systems sometimes are described by the "stretched exponential" expression of the form $N(t) = N(0)\exp(-kt^{\alpha})$, for $\alpha < 1$,[9] or by a power law dependence of the form $N(t) = N(0)/(1 + kt)^{\beta}$, for $\beta > 1$,[10,11] in which k is a characteristic rate constant and $N(t)$ represents an appropriate experimental observable (e.g., population, probability, or number density). Although numerous methods exist for probing motions in biopolymers, and many proteins have been studied in the past few years, whether the dynamics of biopolymers should be interpreted by using correlation times and activation barriers or by using distributed dynamics remains unclear. A central conceptual question is whether fast internal, slow internal, and hydrodynamic diffusional motions are separable or whether strongly coupled dynamical modes and broad distributions of correlation times render such a separation artifactual. Another question is whether enthalpic, entropic, or hydrodynamic considerations are dominant factors in defining motional time scales. These basic questions have been debated extensively for the specific case of heme proteins, and concern about a simple picture involving activated kinetics is warranted.[11,12]

NMR methods for detecting motions in biopolymers often are classified according to time scales. For solution NMR, whether the motions of interest are faster or slower than hydrodynamic rotational diffusion is particularly significant experimentally. For SSNMR, the relevant consideration is whether the motions are faster or slower than the inverse of the (typically quadrupolar or chemical shift) anisotropy. In either case, motions in the nanosecond and picosecond range usually are considered fast and are detected mainly through relaxation rates,[13−16] while those in the microsecond time scale and slower usually are considered intermediate to slow and are probed primarily through line shape analyses, rotating frame relaxation rates, magnetization transfer, and selective inversion recovery methods. The methods by which dynamical parameters should be extracted from NMR relaxation rates and line shapes are under current investigation; these questions are different in flavor

[†] Department of Chemistry.
[‡] Department of Biochemistry and Molecular Biophysics.
[§] Present address: European Molecular Biology Lab, Meyerhoffstrasse 1, D69012 Heidelberg, Germany.
[⊗] Abstract published in *Advance ACS Abstracts,* August 1, 1996.

S0022-3654(96)00611-9 CCC: $12.00

for solution and SSNMR. Progress in these areas also should help in identifying and validating appropriate computational approaches for simulating protein dynamics.

A basic classification of experimental time scales also might correspond to a separation in terms of the types of motions exhibited by simple systems. For example, many motions on the picosecond and nanosecond time scales with small excursion angles are regarded as librations or hindered motions within an energetic well (e.g., amide plane rocking motions), while slower motions are considered as activated processes in which the system must cross some energetic maximum (e.g., aromatic ring flips). Functional relevance of infrequent large angle excursions is underscored by crystallographic studies of ligand gated domain motions and docking process that involve major restructuring of protein conformations. Small angle, higher frequency motions contribute to function by influencing barriers for slower motions and by modulating entropic changes associated with functional processes. Measurements of protein dynamics on fast time scales are plentiful. Slower domain motions have been more sparsely explored: the few measurements that exist are quite exciting because they offer entrée into dynamical processes that are close to the time scales on which docking, catalysis, and release take place. For example, blatant defects in protein and DNA crystal structures, such as the "flipped-out" substrate base in the crystal structure of DNA cytosine-5-methyltransferase,[17] pose intriguing energetic and dynamical issues; development of NMR methods that permit observation of the motions associated with noncanonical structural features is an important objective.

The strengths and weaknesses of solution and solid state NMR spectroscopy are complementary. Solution NMR offers a probe of motions of the entire molecule in an efficient fashion when global isotopic enrichment is feasible; in contrast, the nearly complete lack of spectral resolution of one labeled site from another in static SSNMR spectra of unoriented samples normally makes laborious selective labeling mandatory and data acquisition highly inefficient. On the other hand, overall rotational diffusion in solution averages the anisotropic part of the chemical shift, dipolar and quadrupolar tensors. Hydrodynamic tumbling also dominates the characteristics of the spectral density functions associated with these interactions. Because the anisotropic line shapes are preserved, SSNMR has the potential to dissect motional models to a much greater degree and with rather fewer assumptions. More dramatic dynamical effects from anisotropic interactions are manifest in the absence of rotational diffusion and more experimental constraints for an individual site can be garnered from anisotropic interactions. This review is intended to identify opportunities for strengthening solution and solid state methods for characterizing biomolecular dynamics, individually and collaboratively, that are likely to clarify fundamental physical characteristics and biological functions of biopolymers.

Solution NMR Methods

Investigations of dynamic processes by high-resolution solution-state NMR spectroscopy can be categorized on the basis of the correlation times relevant for experimentally accessible motional processes: (1) laboratory frame nuclear spin relaxation measurements sensitive to picosecond to nanosecond time scales, (2) line shape analysis and rotating frame nuclear spin relaxation measurements sensitive to microsecond to millisecond time scales, and (3) magnetization exchange spectroscopy sensitive to millisecond to second time scales. In each of these experiments, the system remains at chemical equilibrium during the spectroscopic measurement; nonequilibrium rapid mixing and perturbative techniques are not covered. This review focuses on heteronuclear solution NMR methods, rather than homonuclear ^{1}H techniques, because the reduced importance of ^{1}H dipolar cross-relaxation for heteronuclear spin relaxation and the increased resolution afforded by multidimensional heteronuclear NMR spectroscopy are valuable, particularly for investigations of large biological macromolecules. The extant literature is dominated by studies of dynamics in proteins because of the relative ease with which isotopically enriched samples can be prepared; nonetheless, a smaller number of investigations of nucleic acid dynamics have been reported.[18−21] Solution NMR samples typically consist of ∼1 mM solute in 200−600 μL sample volume. Consequently, proteins and other biological macromolecules suitable for investigation must be monodisperse (resistant to nonspecific aggregation), stable for long periods of time, and amenable to isotopic enrichment.

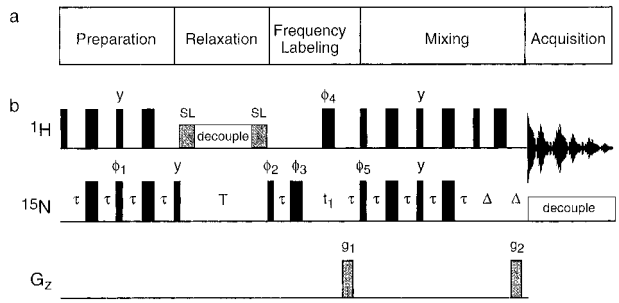

Figure 1. Experimental techniques for NMR spin relaxation measurements. (a) Block diagram illustrating pulse sequences for spin relaxation studies. In some instances the frequency-labeling and relaxation periods are reversed. (b) Sample pulse scheme used to measure ^{15}N R_1 relaxation rate constant using a two-dimensional, proton-detected pulse sequence. The preparation period consists of a refocused INEPT sequence, the relaxation period is an inversion recovery experiment with proton decoupling, and the mixing period is a sensitivity-enhanced reverse INEPT sequence. Thin and thick bars represent 90° and 180° pulses, respectively; SL denotes a purge pulse. The phase cycling is as follows: $\phi_1 = (x,-x)$; $\phi_2 = y$; $\phi_3 = 4(x)$, 4(y), 4($-x$) 4($-y$); $\phi_4 = (x,x,-x,-x)$; $\phi_5 = x$; and receiver $(x,-x,x,-x,-x,x,-x,x)$. The 180° pulses without phase designations are applied along the x-axis. Coherence selection is performed using pulsed field gradients g_1 and g_2; quadrature detection is obtained by inverting g_1 and phase cycling ϕ_2, ϕ_5, and the receiver as described elsewhere.[49] Additional field gradient pulses utilized for artifact suppression are omitted for clarity. The value of τ is set to $1/(4J_{NH})$, and Δ must be longer than g_2 plus a recovery delay. The delay T is parametrically varied in a series of 2D experiments, and the resulting peak intensities are fit to determine the first-order rate constant, R_1. The corresponding sequences for measuring R_2 and the NOE, and sequences adapted to minimize solvent saturation, are given by Farrow et al.[109]

Biological macromolecules often have limited solubility and complex, congested NMR spectra. As a result, two-dimensional NMR spectroscopy is nearly always necessary for studies of biomolecular dynamics, and the sensitivity of the experiments must be maximized. The NMR pulse sequences used for these experiments can be conceptualized as shown in Figure 1; the relevant components of the experiments are as follows:

(1) Preparation: For proton-detected heteronuclear NMR spectroscopy, the preparation period normally consists of a DEPT[22] or INEPT[23,24] polarization or magnetization transfer step from protons to the nucleus of interest; in certain instances, magnetization transfer via the NOE is utilized.[25,26] The polarization transfer step increases the sensitivity of the experiment by as much as γ_H/γ_X (in which X is the heteronucleus of interest; for example, this ratio is ca. 4 for ^{13}C and 10 for ^{15}N); in practice, somewhat smaller enhancements are observed due to pulse imperfections and relaxation effects.[27]

(2) Relaxation: The density operator present after the preparation period provides the initial condition for the relaxation experiment. The relaxation period is similar to one-dimensional relaxation experiments used in small molecules. Relaxation of components of the density operator other than the Bloch longitudinal and transverse magnetizations (such as multiple-quantum coherence, two-spin order, or antiphase magnetization) can be characterized because the subsequent mixing period can effect transfer from nonobservable to observable coherences. The relaxation period is increased parametrically in a time series of two-dimensional (2D) NMR spectra to generate relaxation decay curves[28] or is increased in accordion[29−31] fashion to encode the relaxation rate constant into the line shape of the resonance signals in a single 2D NMR spectrum.

(3) Frequency labeling: Chemical shifts are recorded during the t_1 incrementable delay to generate the indirect dimension of the two-dimensional NMR spectrum.

(4) Mixing: The desired heteronuclear coherence is transferred to proton magnetization using reverse DEPT, INEPT, or sensitivity-enhanced[32,33] polarization transfer sequences; proton detection increases the sensitivity of the experiment by as much as $(\gamma_H/\gamma_X)^{3/2}$.[27]

(5) Acquisition: The relaxation-encoded, frequency-labeled transverse proton magnetization is recorded during t_2.

Two-dimensional Fourier transformation yields a 2D frequency domain spectrum in which the relaxation decay is encoded in the intensities (parametric variation) or line shape (accordion variation) of the two-dimensionally resolved resonance signals. Multiple relaxation mechanisms for a single nucleus and correlated interactions for different nuclei lead to multiexponential relaxation decays. Resolving multiexponential decays by nonlinear least-squares fitting is difficult because of the limited sensitivity of NMR spectroscopy. Accordingly, experimental techniques that generate monoexponential decays are preferred whenever possible. For example, cross-correlation between chemical shift anisotropy (CSA) and dipolar relaxation mechanisms can be suppressed by appropriately designed radio-frequency (rf) pulse trains,[34−36] and multiple spin correlation effects in methyl groups can be minimized by use of deuterium, rather than ^{13}C or ^{1}H, NMR spectroscopy.[37,38]

Fast Time Scale Dynamics. Techniques for investigating fast dynamics (10^{-12} to 10^{-8} s) in biological macromolecules most commonly utilize the dipolar, chemical shift anisotropy (CSA), and quadrupolar relaxation mechanisms.[39] A spin relaxation investigation of a macromolecule generates a set of relaxation rate constants for nuclei distributed throughout the molecule. Relaxation rate constants are interpreted within the framework of Bloch−Wangsness−Redfield (BWR) relaxation theory[13] (*vide infra*). In the most common protocol,[26,40] the inversion-recovery technique[41] is used to measure the spin−lattice relaxation rate constant for longitudinal magnetization, R_1; the Carr−Purcell−Meiboom-Gill (CPMG) technique[42,43] is used to measure the spin−spin relaxation rate constant for transverse magnetization, R_2; and the steady-state NOE technique[44] is to measure the NOE $= 1 + \sigma/R_1$, in which σ is the heteronuclear cross-relaxation rate constant. The relaxation rate constant in the rotating reference frame, $R_{1\rho}$, can be measured as an alternative to the R_2 measurement.[45] In the absence of chemical exchange (*vide infra*) $R_2 = R_{1\rho}$ in biological macromolecules. The data can be expanded to include relaxation rate constants for longitudinal two spin order or antiphase coherences.[46] The data can be expanded further by measuring rate constants at different static magnetic field strengths.[47,48]

Experimental methods have been developed extensively and applied widely for ^{15}N relaxation measurements of backbone and side chain ^{15}N nuclear spins in proteins.[28,49,50] Experimental techniques have been developed for measurements of spin relaxation of protonated ^{13}C nuclei in naturally abundant,[51−53] fractionally enriched,[54] and fully enriched samples.[55,56] Other techniques have been reported for ^{13}C spin relaxation in carbonyl groups,[57] in semideuterated ^{13}CHD methylene moieties,[58] and in methyl groups.[25,59] Heteronuclear cross-polarization has been incorporated into techniques for measuring ^{31}P and ^{113}Cd spin relaxation.[60] Relaxation measurements for $^{13}CH_2D$ methyl groups have been developed in a particularly elegant manner to characterize deuterium quadrupolar relaxation rate constants: separate measurements of the relaxation of $I_zS_zD_z$, $I_zS_zD_x$, and I_zS_z coherences (D = ^{2}H, I = ^{1}H, and S = ^{13}C) allow determination of the pure deuterium $R_1 = R(I_zS_zD_z) - R(I_zS_z)$ and $R_2 = R(I_zS_zD_x) - R(I_zS_z)$, in which $R(A)$ designates the relaxation rate constant of coherence A.[37,38] Considerable development of the experimental techniques has occurred in order to address dipolar-CSA cross-correlation,[34−36] polarization transfer in methyl groups,[25,59] ^{13}C−^{13}C scalar and dipolar interactions in ^{13}C-enriched molecules,[55] solvent saturation transfer in {^{1}H}−^{15}N NOE measurements,[61−63] and ^{1}H, ^{13}C, and ^{2}H interactions in fractionally deuterated molecules.[37,38]

For dipolar, chemical shift anisotropy (CSA), and quadrupolar relaxation mechanisms, BWR theory, outlined in the discussion of SSNMR (*vide infra*), leads to classic formulas that express relaxation rate constants as linear combinations of spectral density functions, $J(\omega)$, at characteristic frequencies.[64] For example, the dipolar interaction between an X (=^{13}C or ^{15}N) spin and a ^{1}H spin and the CSA interaction of the X spin result in the following equations for the relaxation rate constants of the X spin (assuming that cross correlations between the interactions have been suppressed experimentally):

$$R_1 = (d^2/4)[J(\omega_H - \omega_X) + 3J(\omega_X) + 6J(\omega_H + \omega_X)] + c^2J(\omega_X) \quad (1)$$

$$R_2 = (d^2/8)[4J(0) + J(\omega_H - \omega_X) + 3J(\omega_X) + 6J(\omega_H) + 6J(\omega_H + \omega_X)] + (c^2/6)[4J(0) + 3J(\omega_X)] \quad (2)$$

$$\sigma = (d^2/4)[6J(\omega_H + \omega_X) - J(\omega_H - \omega_X)] \quad (3)$$

in which $d = (\mu_0 h\gamma_X\gamma_H/8\pi^2)\langle r_{XH}^{-3}\rangle$, $c = \Delta\sigma\omega_X/\sqrt{3}$, μ_0 is the permeability of free space, h is Planck's constant, γ_H and γ_X are the gyromagnetic ratios of ^{1}H and X, respectively, r_{XH} is the X−H bond length, ω_H and ω_X are the Larmor frequencies of ^{1}H and X, respectively, $\Delta\sigma$ is the CSA of the X spin, and chemical shift tensor is assumed to be axially symmetric. The spectral density function is given by

$$J(\omega) = {}^{1}/_{5}\int_0^\infty < P_2[\mu(0)\cdot\mu(t)] > \cos(\omega t)\, dt \quad (4)$$

in which $\mu(t)$ is a unit vector defining the orientation of the unique axis of the relaxation interaction ($\mu(t)$ is parallel to the internuclear vector for dipolar-coupled nuclei and the symmetry axis of axially symmetric CSA or quadrupolar tensors) in the laboratory reference frame, $P_2[x]$ is the second Legendre polynomial, and $\langle\ \rangle$ represents an ensemble average. The spectral density function is determined by overall rotational diffusion of the protein and by intramolecular motions of $\mu(t)$. For amide ^{15}N spins and aliphatic ^{13}C spins, the bond vector and the unique axis of the chemical shift tensor are nearly collinear.

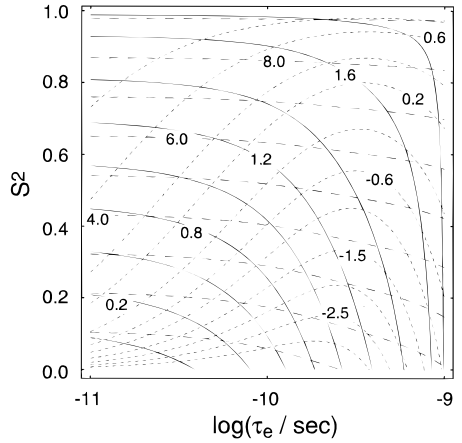

Figure 2. Dependence of ^{15}N R_1, R_2, and the NOE on model-free parameters S^2 and τ_e. (—) R_1 contour lines are drawn at 0.2, 0.4, 0.6, 0.8, 1.0, 1.2, 1.4, 1.6, and 1.7 s^{-1}; (— — —) R_2 contour lines are drawn at 1.0, 2.0, 3.0, 4.0, 5.0, 6.0, 7.0, 8.0, and 9.0 s^{-1}. (- - -) NOE contour lines are drawn at −3.0, −2.5, −2, −1.5, −1.0, −0.6, −0.2, 0.2, 0.4, 0.6, and 0.7. A subset of the contours are labeled for clarity. Calculations were performed for $\tau_m = 8$ ns.

Data analysis proceeds by one of four approaches: (i) functional forms for $J(\omega)$ derived from specific physical motional models are fit to the data,[39,65,66] (ii) simple "model-free" functional forms for $J(\omega)$ containing a limited number of free parameters are fit to the data,[67−69] (iii) $J(\omega)$ is derived from numerical computations that have been parametrized to reproduce the experimental data,[70] and (iv) $J(\omega)$ is determined directly from the experimental data by "spectral density mapping".[46,71,72] The model-free and spectral density mapping techniques have been most widely applied to biomolecules in the past few years.

The "model-free" Lipari−Szabo formalism[67,68] or variants of this approach[69] describes internal dynamics in terms of correlation times and order parameters. The original model-free formalism[67,68] utilized the spectral density function

$$J(\omega) = (1/5)[S^2\tau_m/(1 + \omega^2\tau_m^2) + (1 - S^2)\tau/(1 + \omega^2\tau^2)] \quad (5)$$

in which τ_m is the isotropic overall rotational correlation time of the protein, S^2 is the square of the generalized order parameter characterizing the equilibrium distribution of orientations in a molecular reference frame, τ_e is the effective internal correlation time for internal motions, and $\tau = (1/\tau_m + 1/\tau_e)^{-1}$. For simplicity, S^2 will be referred to as the order parameter in the following. The model-free formalism is essentially identical to the "two-step" model proposed by Halle and Wennerström.[73] The dependence of R_1, R_2, and the NOE on S^2 and τ_e is illustrated in Figure 2. The extended two-time scale model spectral density function proposed by Clore et al.[69] is useful, particularly for sites exhibiting complex dynamic properties. In this model

$$J(\omega) = (1/5)S_f^2[S_s^2\tau_m/(1 + \omega^2\tau_m^2) + (1 - S_s^2)\tau/(1 + \omega^2\tau^2)] \quad (6)$$

in which S_f^2 is the order parameter for motions on a very fast time scale ($\tau_f < 10$ ps), and S_s^2 is the order parameter for motions on a intermediate time scale $\tau_f \ll \tau_e \ll \tau_m$.

Model-free parameters are determined from experimental relaxation rate constants by nonlinear minimization of a χ^2 variable.[53] Frequently, a phenomenological exchange rate constant must be simultaneously fit to account for chemical exchange contributions to the R_2 or $R_{1\rho}$ experiments (*vide infra*).[40] Parsimonious subsets of model-free parameters necessary to fit the experimental data can be determined heuristically[40,74] or by using F-statistical testing.[75] The accuracy of the motional parameters calculated from the relaxation data using the model-free formalism has been discussed.[68,76] S^2 is well-determined by NMR relaxation measurements. However, as eqs 5 and 6 make clear, the spectral density function does not contain information on internal motions significantly slower than rotational diffusion,[67,68] and τ_e can only be characterized precisely over a relatively narrow range. In most cases, $\tau_e <$ 30 ps and $\tau_e \rightarrow \tau_m$ are very poorly determined.

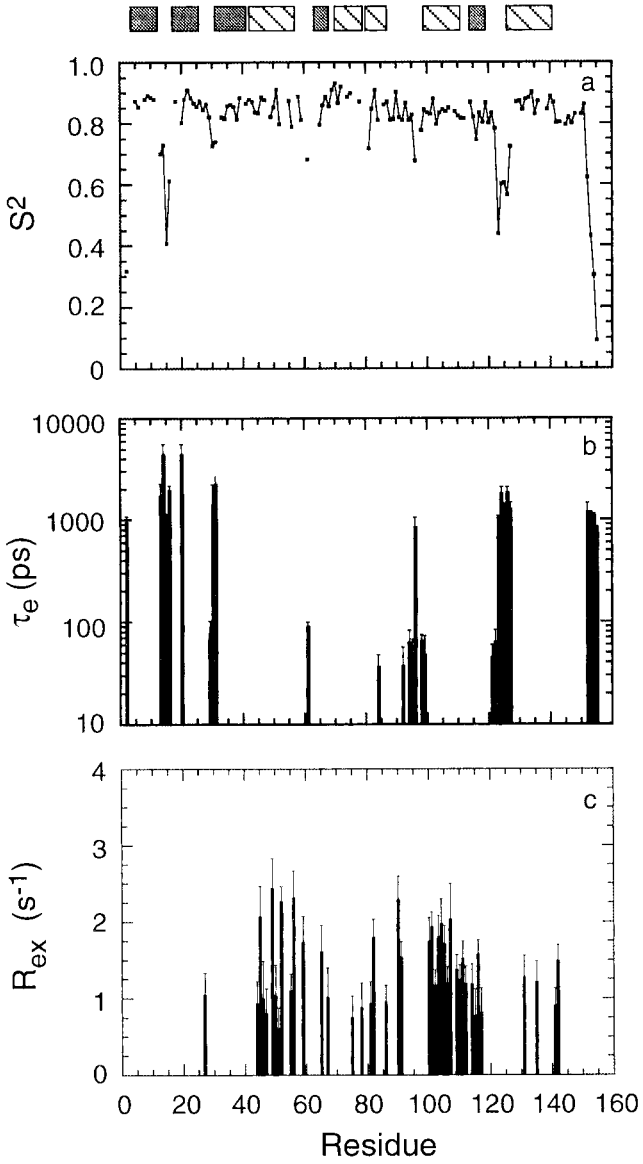

Figure 3. Model-free analysis for *E. coli* RNase H.[75] Backbone amide (a) model-free S^2, (b) model-free τ_e, and (c) exchange terms R_{ex} are illustrated as a function of amino acid residue number. Stippled bars indicate the positions of the β-strands, and hatched bars indicate the positions of the α-helices in RNase H. Data were calculated from ^{15}N R_1, R_2, and NOE measurements obtained at 300 K and a magnetic field strength of 11.74 T. Values of R_2 were determined by using a CPMG experiment with $\tau_{CPMG} = 1.2$ ms.

Typical experimental model-free parameters for backbone ^{15}N amide spins are illustrated for the *Escherichia coli* protein ribonuclease H (RNase H) at 300 K in Figure 3.[75] At this temperature, $\tau_m = 9.3$ ns. As in other proteins, backbone ^{15}N order parameters for canonical secondary structure elements are $S^2 \sim 0.86$; order parameters for loops and termini are reduced. Uncertainties in S^2 are typically 0.01−0.04. Values for τ_e are

less well determined with uncertainties frequently on the order of 25%−50%. Relatively rigid sites ($S^2 > 0.75$) generally have $\tau_e < 100$ ps; values of τ_e for the slower time scale in the extended model free formalism of eq 6 are typically 1−4 ns. Model-free parameters have been reported for RNase H at 285, 300, and 310 K.[77] A modest decrease in the mean order parameter from 0.88 to 0.85 over this temperature range is consistent with limited increases in the conformational space accessible to the $^1H-^{15}N$ bond vector within a single potential energy well or a series of wells separated by very low energy barriers. While backbone dynamics of more than 20 proteins have been reported, more limited results are available for the dynamics of side chains.[78−80] A general tendency for the order parameters of side chain spins to be correlated with solvent accessibility has been observed,[75,78] but local electrostatic and hydrogen-bonding interactions also are expected to modulate the motional properties of side chains. Identification of functional changes in side chain dynamics as a result of ligation, catalysis, or other process is a critical area for future development.[80−83]

The square of the order parameter is a measure of the equilibrium distribution of orientations of the vector $\mu(t)$ in a molecular reference frame and ranges from unity for vectors with fixed orientations to zero for vectors with isotropic orientational distributions. For small-amplitude, axially symmetric orientational distributions,

$$S^2 = 1 - {}^3/_2\langle\theta^2\rangle \tag{7}$$

in which $\langle\theta^2\rangle$ is the mean-square polar angle. If motion of $\mu(t)$ is modeled as restricted diffusion in a cone, then S^2 is given by[67]

$$S^2 = [\cos\theta_0(1 + \cos\theta_0)/2]^2 \tag{8}$$

and the amplitude of motion is characterized by the cone semiangle, θ_0. In an alternative conceptualization, the Gaussian axial fluctuation model,[84] the vector diffuses within a parabolic potential on the surface of a cone and S^2 is given by

$$S^2 = 1 - 3\sin^2\theta\{\cos^2\theta(1 - \exp[-\sigma_f^2]) + 0.25\sin^2\theta(1 - \exp[-4\sigma_f^2])\} \tag{9}$$

in which θ is the (fixed) angle between $\mu(t)$ and the director axis for the motion and σ_f is the standard deviation of the fluctuation in the azimuthal angle. If $\sigma_f \rightarrow \infty$, then $S^2 = (P_2[\cos\theta])^2$ is the result for unrestricted diffusion on the surface of a cone.[85] For rapid jumps of the bond vector between N distinct orientations, the order parameter is[67]

$$S^2 = \sum_{i,j=1}^{N} p_i p_j P_2(\cos\theta_{ij}) \tag{10}$$

in which p_i is the equilibrium population of vectors having the ith orientation and θ_{ij} is the angle between vectors having the ith and jth orientations. The canonical $S^2 \sim 0.86$ found for ^{15}N amide spins in secondary structure elements corresponds to a root-mean-square angular fluctuation $\langle\theta^2\rangle^{1/2} = 12°$, using eq 7; a diffusional libration within a cone of semiangle $\theta_0 = 18°$, using eq 8; a torsional libration of the backbone ϕ dihedral angle with $\sigma_\phi = 14°$, using eq 9; or a jump between two sites with $\theta_{12} = 26°$, using eq 10 for $N = 2$ and $p_1 = p_2 = 0.5$.

Changes in S^2 upon ligand binding or conformational transition in a biological macromolecule reflect altered flexibility and consequent changes in conformational entropy. Model-free analyses have been reported for a number of proteins in unligated and ligated states, including backbone ^{15}N measurements for calbindin D_{9k},[86] the immunophilin FKBP-12,[87,88] ribonuclease T1,[89] and HIV protease.[90] Leucine methyl dynamics have been characterized by ^{13}C spin relaxation of staphylococcal nuclease (SNase) in the unbound state and in a complex with thymidine 3′,5′-bisphosphate and Ca^{2+}.[81] In these systems, order parameters for residues located in or near the ligand binding site are increased upon complex formation by as much as 0.20. Order parameters can be used to estimate an upper bound for the change in Gibbs free energy resulting from conformational restriction:[91]

$$\Delta G = -kT\sum_n \ln\left(\frac{1 - S_{n^2}{}^2}{1 - S_{n^1}{}^2}\right) \tag{11}$$

in which $1 - S_{nk}{}^2$ is the order parameter for the nth spin in the kth state and the summation extends over all affected nuclei. A similar formalism enables the configurational entropy to be calculated directly, and the theoretical results have been compared to results derived from a molecular dynamics simulation of RNase H.[92] Equation 11 suggests that fast time scale dynamics impose a conformational entropic free energy penalty if a ligand binding site is rigidified in the ligated state. The increase in S^2 observed upon ligation of Ca^{2+} by calbindin D_{9k} corresponds to $\Delta G = 0.4$ kcal/mol per affected amide group.

A comprehensive study of the dynamical properties of C-terminal SH2 domain of phospholipase C-γ1 in the presence and absence of a phosphotyrosine peptide ligand has been performed by Kay and co-workers, including backbone ^{15}N dynamics,[49] ^{15}N relaxation measurements for Arg N^ϵ,[80] ^{13}C $R_{1\rho}$ measurements for Arg C^ζ spins,[80] and methyl side chain dynamics measured using deuterium relaxation.[82] Complex patterns of dynamics on multiple time scales for backbone and side chain residues suggest that, at least for this one example, binding a relatively flexible macromolecular ligand may have different consequences for protein dynamics than binding of small rigid ligands and metal ions.

The assumption of a single isotropic rotational correlation time (cf eqs 5 and 6) is a simplification for most macromolecules. In principle, extensions to the model-free formalism that include anisotropic overall rotational diffusion[67,73,76] must be applied in the analysis of relaxation data;[93,94] however, the effects are small for slightly nonspherical, globular proteins.[75,95] More fundamentally, the anisotropy of the diffusion tensor can be altered by allosteric or ligand binding processes. Experimental characterization of the diffusion tensor by NMR spectroscopy can be used to test hydrodynamic models for the protein or protein complex. If τ_e and $(1 - S^2)$ are small, then $J(\omega) = S^2J_0(\omega)$, in which $J_0(\omega)$ is the spectral density function for overall rotational motion. Consequently,

$$R_2/R_1 = \{4J_0(0) + J_0(\omega_H - \omega_X) + 3J_0(\omega_X) + 6J_0(\omega_H) + 6J_0(\omega_H + \omega_X) + [4c^2/(3d^2)][4J_0(0) + 3J_0(\omega_X)]\}/\{2J_0(\omega_H - \omega_X) + 6J_0(\omega_X) + 12J_0(\omega_H + \omega_X)] + [8c^2/d^2)]J_0(\omega_X)\} \tag{12}$$

is independent of internal motions. For isotropic or axially symmetric diffusion tensors, $J_0(\omega)$ is given by[96]

$$J_0(\omega) = \frac{2\tau_m}{5(1 + \omega^2\tau_m^2)} \quad \text{(isotropic)}$$

$$J_0(\omega) = \frac{2}{5}\sum_{i=0}^{2} A_i \frac{\tau_i}{1 + \omega^2\tau_i^2} \quad \text{(axially symmetric)} \quad (13)$$

in which $\tau_m = (6D)^{-1}$, $D = (D_{||} + 2D_\perp)$ is the isotropic diffusion constant, $D_{||}$ and $D_\perp$ are the components of an axially symmetric diffusion tensor, $\tau_i^{-1} = 6D_\perp - i^2(D_\perp - D_{||})$, $A_0 = (3\cos^2\theta - 1)^2/4$, $A_2 = 3\sin^2\theta\cos^2\theta$, $A_3 = (3/4)\sin^4\theta$, and θ is the angle between the X−H bond vector and the unique axis of the diffusion tensor. If the three-dimensional structure of the macromolecule is known, the principal components and orientation of the diffusion tensor can be obtained by a global optimization of eq 13 for all nuclei. This technique has been applied to ubiquitin,[95] trp repressor,[94] and the c-Jun leucine zipper.[93] The results for $D_{||}/D_\perp$ are 1.17 (ubiquitin), 1.29 (trp repressor), and 1.79 (c-Jun) and are in good agreement with hydrodynamic calculations. The same analysis is applicable to a fully anisotropic diffusion tensor; however, for ubiquitin and trp repressor, the anisotropic model is not a statistically significant improvement to the axially symmetric model. (A fully anisotropic model was not fit to the c-Jun data.) These molecules are expected to have nearly axially symmetric diffusion tensors, based on calculations of the inertia tensors from the three-dimensional structures of the molecules. In an alternative approach, the model-free formalism is used to determine values of S^2, τ_e, and a local τ_m independently for each residue. The variation in the local values of τ_m, together with bond vector orientations derived from a high-resolution structure, is used to determine the diffusion tensor by a linear analysis.[97] Fully anisotropic diffusion tensors were reported for each zinc finger module in a three-finger protein, and a model for the relative orientations of the individual domains was presented.[97] Diffusion anisotropy also has been used to evaluate hydrodynamic models for calmodulin.[98] These methods hold considerable promise for detailed investigations of the hydrodynamic properties of biological macromolecules.

Although the model-free formalism is a succinct and tractable method for the analysis of NMR spin relaxation data, significant practical and interpretive issues remain unresolved:

(1) Equation 5 is exact for sufficiently fast internal motions, $\omega\tau_e \ll 1$; outside of this limit, the degree to which eqs 5 and 6 approximate the macromolecular spectral density function is difficult to establish. Values of $J(\omega)$ calculated from the model-free formalism and from spectral density mapping of eglin *c*[47] (*vide infra*) show small, but systematic, differences; notably, the spectral density function derived from direct mapping decays slightly slower than the model spectral density functions.

(2) Values of τ_e are difficult to measure precisely and are difficult to interpret.

(3) Microscopic physical models for internal motions cannot be determined directly from the model-free parameters. Fast time scale motions (τ_e < 100 ps) are amenable to molecular dynamics simulations[99−103] or normal mode analysis;[100,104] however, for slower motions (τ_e > 100 ps), S_s^2 and τ_e reflect motions that are inadequately sampled during 500 ps−1 ns simulations and are poorly represented within a harmonic approximation.

(4) The Lipari−Szabo approach makes the implicit assumption that the internal motions can be treated as a convergent sum of exponentials; the association between time constants and physical processes can be cloudy in many instances, particularly if the motional model does not converge well in an exponential basis set. The Lipari−Szabo approach to descriptions of rapid internal dynamics in DNA has been criticized,[105] in part because it appears to provide an inadequate description of internal dynamics, such as twisting or bending of a rodlike polymer.

In spectral density mapping, the characteristic values of $J(\omega)$ are determined directly from relaxation data. In the original version of this approach,[46,106] R_1, R_2, σ, the rate constant for relaxation of heteronuclear antiphase coherence, and the rate constant for relaxation of two-spin longitudinal order are measured. As a practical matter, the latter two coherences cross-relax with remote ^{1}H spins, and the ^{1}H spin−lattice relaxation rate constant also must be measured. Proton spin−lattice relaxation is multiexponential, and determining the ^{1}H spin−lattice relaxation rate constant accurately is problematical. The values of $J(\omega)$ at the characteristic frequencies are determined from the relaxation data by inversion of the resulting linear system of equations (e.g. eqs 1−3). Determining accurate values for $J(\omega_H)$, $J(\omega_H + \omega_N)$, and $J(\omega_H - \omega_N)$ is difficult both because of inaccuracies in the ^{1}H relaxation rate constants and because the system of equations is close to singular. For ^{15}N spin relaxation $\gamma_N/\gamma_H = 0.101$ and $J(\omega_H \pm \omega_N) \approx J(\omega_H)$. Under this assumption, values of $J(0)$, $J(\omega_N)$, and $J(\omega_H)$ can be obtained simply from R_1, R_2, and σ (or NOE) without recourse to relaxation rate constants for antiphase coherence, two-spin order, and ^{1}H magnetization. This approach and its variants have been called reduced spectral density mapping[47,71] or quasi-spectral density analysis.[72,107] In a particularly elegant version,[71] the linear combinations of $J(\omega_H - \omega_N)$, $J(\omega_H)$, and $J(\omega_H + \omega_N)$ that appear in eqs 1−3 are approximated to first order by a single term of the form $\alpha J(\beta\omega_H)$, in which α and β are constants. The resulting dipolar and CSA relaxation rate constants are given by

$$R_1 = (d^2/4)[3J(\omega_N) + 7J(0.921\omega_H)] + c^2 J(\omega_N) \quad (14)$$

$$R_2 = (d^2/8)[4J(0) + 3J(\omega_N) + 13J(0.955\omega_H)] + (c^2/6)[4J(0) + 3J(\omega_N)] \quad (15)$$

$$\sigma = (5d^2/4)J(0.870\omega_H) \quad (16)$$

The system of equations can be solved for $J(0)$, $J(\omega_N)$, and $J(0.870\omega_H)$ in three ways: (1) Assume $J(0.870\omega_H) = J(0.921\omega_H) = J(0.955\omega_H)$. (2) Assume $J(\epsilon\omega_H) = (0.870/\epsilon)^2 J(0.870\omega_H)$. (3) Assume $J(\epsilon\omega_H) = J(0.870\omega_H) + (\epsilon - 0.870)\omega_H J'(0.870\omega_H)$, in which $J'(0.870\omega_H)$ is the first derivative of $J(\omega)$ evaluated at $0.870\omega_H$. The derivative is estimated by a difference equation using data acquired at two magnetic field strengths. Figure 4 illustrates reduced spectral mapping for the proteinase inhibitor eglin c using method (1) and data acquired at magnetic field strengths of 7.04, 11.74, and 14.1 T.

Although spectral density mapping obviates concerns over whether the model-free formalism provides an appropriate model spectral density function, significant difficulties in interpretation remain: (1) The paucity of magnetic fields available precludes comprehensive characterization of the (continuous) spectral density function by a limited set of discrete values. (2) Separation between internal and overall motional contributions to the spectral density function is not obtained naturally. (3) Chemical exchange contributions to R_2, $R_{1\rho}$, and the rate constant for antiphase magnetization are difficult to quantify in the absence of data at multiple field strengths (*vide infra*). (4) The otherwise useful constraint that the area under the spectral density function is constant because the correlation function is normalized does not hold if significant contributions to $J(0)$ arise

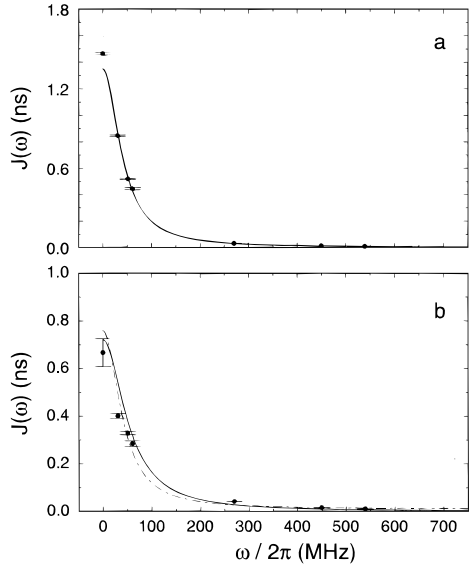

Figure 4. Spectral density analysis for eglin *c*.[47] Experimental $J(\omega)$ for backbone ^{15}N nuclei of (a) Arg 22 and (b) Asp 46 determined by using the reduced spectral density mapping technique and relaxation data acquired at static magnetic field strengths of 7.04, 11.74, and 14.1 T and a temperature of 309 K. The solid and dashed lines represent the best fits of the data to eqs 5 and 6, respectively. Solid and dashed lines are indistinguishable in (a). Arg 22 is located in an α-helix, and Asp 46 is located in the binding loop.

from chemical exchange. (5) Modeling may still be required to provide a microscopic, quantitative interpretation of the results.

While the existing experiments and analytical procedures are fairly robust for compact globular proteins, a number of studies have been reported for partially unfolded or otherwise non-native proteins: basic pancreatic trypsin inhibitor (BPTI),[108] the drk SH3 domain,[109] the immunoglobulin binding domain of protein G,[110] SNase,[111,112] and chymotrpsin inhibitor 2.[113] In these instances, very complex dynamics can be observed on multiple time scales. Further development of experimental and theoretical techniques for investigating such systems is necessary.

Intermediate Time Scale Dynamics. In contrast to fast time scales, relatively few experiments for measuring motions on intermediate microsecond to millisecond time scales have been developed or applied to proteins. On these time scales, conformational or chemical exchange renders the environment, and consequently the chemical shift, of affected nuclei time dependent. Herein, the intermediate time scale is defined by the requirement that the chemical exchange process be in the fast exchange limit, in which single, population-averaged resonance lines are observed for the exchanging chemical species. Slow exchange, in which resolved resonance lines are observed for each exchanging chemical species, is discussed below. For simplicity, only exchange between two magnetic environments is considered in the following; more complex kinetics are treatable as described for SSNMR (*vide infra*). A single resonance line with a population weighted-average apparent chemical shift, $\bar{\omega}_0 = p_1\omega_1 + p_2\omega_2$, is observed in the NMR spectrum if $\tau_{ex}|\Delta\omega| < 1$, in which $\Delta\omega = \omega_2 - \omega_1$ is the difference in chemical shift of the nucleus in the multiple environments, $\tau_{ex} = p_1/k_{-1} = p_2/k_1$, p_1 and $p_2 = 1 - p_1$ are the populations of the two conformational states, k_1 is the forward reaction rate constant, and k_{-1} is the reverse reaction rate constant. Exchange on the $10^{-6}-10^{-3}$ s time scale is manifested as an increased contribution, R_{ex}, to the phenomenological R_2 in a free-precession NMR spectrum (or contribution R_{ex}/π to the line width), in a CPMG experiment,[114] or in a $R_{1\rho}$ experiment.[115] For exchange between two sites R_{ex} is given by[116,117]

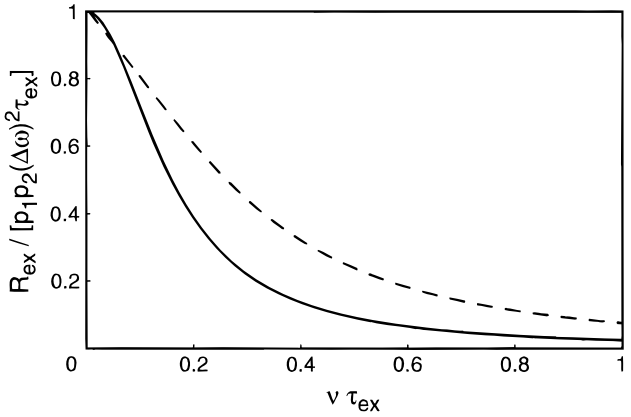

Figure 5. Chemical exchange rate constants. (− − −) Dependence of R_{ex} on $\nu = 1/\tau_{CPMG}$ and the chemical exchange time, τ_{ex}, in a CPMG experiment, as given by eq 18. (—) Dependence of R_{ex} on $\nu = \omega_e/(2\pi)$ and the chemical exchange time, τ_{ex}, in an $R_{1\rho}$ experiment, as given by eq 19. The CPMG curve is accurate for $(p_1p_2)^{1/2}\,|\Delta\omega|\tau_{ex} < 0.2$.

$$R_{ex} = p_1p_2\Delta\omega^2\tau_{ex} \quad \text{(free precession)} \tag{17}$$

$$R_{ex} = \frac{1}{2\tau_{ex}} - \frac{1}{\tau_{CPMG}}\sinh^{-1}\left[\frac{1}{\tau_{ex}\xi}\sinh(\tau_{CPMG}\xi/2)\right] \quad \text{(CPMG)} \tag{18}$$

$$R_{ex} = (\Delta\omega)^2p_1p_2\tau_{ex}/(1 + \tau_{ex}{}^2\omega_e{}^2) \quad (R_{1\rho}) \tag{19}$$

in which τ_{CPMG} is the delay between 180° pulses in the spin echo sequence, $\xi^2 = \tau_{ex}{}^{-2} - 4p_1p_2(\Delta\omega)^2$, $\omega_e = (\Omega^2 + \omega_1{}^2)^{1/2}$, $\Omega = \bar{\omega}_0 - \omega_{rf}$, ω_{rf} is the transmitter radio frequency, and $\omega_1 = \gamma B_1$ is the rf field strength. The free-precession limit is obtained for $\tau_{CPMG} \rightarrow \infty$ or $\omega_e \rightarrow 0$. Equation 18 is an accurate approximation provided $(p_1p_2)^{1/2}|\Delta\omega|\ \tau_{ex} < 0.2$; expressions valid for all time scales are given by Allerhand.[117] The dependence of R_{ex} on τ_{CPMG} or ω_e is illustrated in Figure 5. Equations 17−19 demonstrate that chemical and conformational exchange processes can be detected by NMR spectroscopy only if $|\Delta\omega| > 0$ and that R_{ex} depends quadratically on the static magnetic field strength. While line shape analysis of the free-precession NMR spectrum is an established technique for studying exchange, CPMG and $R_{1\rho}$ experiments have the advantage that τ_{CPMG} and ω_e provide additional variables under experimental control.

Because R_2 (or $R_{1\rho}$) is measured as one of the suite of experiments used to measure fast time scale dynamics (*vide supra*), R_{ex} can be observed as an anomalous increase in R_2 relative to that predicted for dipolar, CSA, or quadrupolar relaxation mechanisms (e.g. eq 2). Interpretation of these exchange terms or determination of the microscopic exchange rates has proven difficult because the relative populations and chemical shift differences for conformers are rarely known. Typical results for R_{ex} obtained using a CPMG experiment with $\tau_{CPMG} = 1.2$ ms are illustrated in Figure 3 for the backbone ^{15}N spins of *E. coli* RNase H. Values of R_{ex} obtained range from 1 to 2.5 s^{-1}. In the fast exchange limit, $\tau_{ex} = R_{ex}/[p_1p_2(\Delta\omega)^2]$. Assuming $p_1 = p_2 = 0.5$ and $\Delta\omega = 320-640$ s^{-1} ($\Delta\delta = 1-2$ ppm), then $\tau_{ex} \approx 10-100$ μs. Mandel et al. have determined the R_{ex} contributions to R_2 (measured using the CPMG technique) for RNase H at 285, 300, and 310 K.[77] The values of R_{ex} increase as the temperature is decreased, which confirms that the motions occur on a time scale faster than τ_{CPMG}.

In principle, a more complete analysis can be performed by measuring R_{ex} as a function of τ_{CPMG} in the CPMG experiment or as a function of ω_e in the $R_{1\rho}$ experiment. While these are well-established techniques for small molecules, application of these techniques to biological macromolecules has proven difficult for the following reasons:[90,114,118] (1) In a CPMG experiment, the minimal value of τ_{CPMG} is limited by sample heating, maximum amplifier duty cycles, and mixing of R_1 and R_2 relaxation rates during the refocusing pulses. (2) In a CPMG experiment the maximum value of τ_{CPMG} is limited by the requirement that $\mathrm{sinc}(\pi J_{XH}\tau_{CPMG}) \rightarrow 1$, in which J_{XH} is the scalar coupling constant, to preclude significant proton−proton relaxation during the spin-echo period.[36] (3) In a spin-locking experiment, the maximum value of ω_1 is limited by sample heating. (4) In a spin-locking experiment, the apparent $R_{1\rho}$ rate constant is given by

$$R_{1\rho} = R_1 \cos^2 \theta_e + R_2 \sin^2 \theta_e + R_{ex} \sin^2 \theta_e \qquad (20)$$

in which $\theta_e = \arctan(\omega_1/\Omega)$ is the "tilt angle" between the directions of the reduced static field and ω_e The value of θ_e differs for every environment experienced by each nucleus in the molecule and varies as ω_1 and ω_{rf} are altered. As a result of the above considerations, the range of accessible τ_{CPMG} values is limited to ca. 0.4−1.5 ms; spin-locking field strengths are limited ca. $\omega_1 = 4$ kHz, and conventional $R_{1\rho}$ measurements can only be performed for spins resonant with the rf field (preventing global examination of biological macromolecules).

Szyperski et al.[119] used variation of ω_1 in a ^{15}N $R_{1\rho}$ experiment to characterize conformational exchange of the backbone amide groups of Cys 38 and Arg 39 in BPTI at 309 K. The transmitter was nearly resonant with both spins, so that θ_e varied only between 80° and 90°. The results indicate that Cys 38 and Arg 39 participate in a chemical exchange process characterized by correlation times of 2.4 ± 1.8 and 1.3 ± 0.5 ms. At 277 K, the exchange process is in the slow limit, and $\Delta\omega$ was measured as 540 s^{-1} for Cys 38 and 1150 s^{-1} for Arg 39.[120] Using these values, the relative population of the major conformer was calculated as 0.84 for Cys 38 and 0.96 for Arg 39. The exchange process was attributed to isomerization of the Cys 14−Cys 38 disulfide bond.

Chemical exchange contributions in eglin *c* at 309 K have been characterized by application of the spectral density mapping technique to data acquired at multiple static magnetic fields using an $R_{1\rho}$ experiment with constant values of ω_{rf} and ω_1.[47] As shown by eqs 17−19, R_{ex} is expected to scale quadratically with the static field strength; consequently,[47,71]

$$J_e(0) = J(0) + 6R_{ex}/(3d^2 + 4c^2) = J(0) + 6\omega_N{}^2\Phi/(3d^2 + 4c^2) \quad (21)$$

in which $J_e(0)$ is the experimentally determined value, $J(0)$ is the value of the spectral density function for dipolar and CSA relaxation, and $\Phi = R_{ex}/\omega_N{}^2$. Values of $J(0)$ and Φ are obtained by curve fitting as a function of $w_N{}^2$. Statistically significant values of Φ ranging from $(9.0 \pm 1.1) \times 10^{18}$ to $(10.7 \pm 2.6) \times 10^{18}$ s were observed for Lys 8, Arg 53, Gly 59, Thr 60 and Asn 64. Assuming $\Delta\omega = 1$ ppm and $p_1 = p_2 = 0.5$, then τ_{ex} is approximated to lie in the range $28 < \tau_{ex} < 40$ μs.

Recently, a new experiment was proposed for measuring an admixture of R_1 and off-resonance $R_{1\rho}$ in a constant-relaxation-time period, *T*. If R_1 relaxation mechanisms operate for a period $T - t$ and $R_{1\rho}$ relaxation mechanisms operate for a period *t*, the relaxation decay curve as a function of *t* yields a phenomenological decay constant:[121]

$$\begin{aligned} R_{eff} &= R_{1\rho} - R_1 \\ &= R_1 \cos^2 \theta_e + R_2 \sin^2 \theta_e + R_{ex} \sin^2 \theta_e - R_1 \\ &= (R_2 - R_1 + R_{ex}) \sin^2 \theta_e \end{aligned} \qquad (22)$$

The resonance offset dependence is reduced to a scaling factor $\sin^2 \theta_e$ that is determined solely by the known parameters ω_{rf}, ω_1, and $\bar{\omega}_0$. R_{eff} is measured in a series of off-resonance experiments by keeping ω_1 constant and shifting ω_{rf} to vary ω_e. Values of τ_{ex} and $p_1p_2\Delta\omega^2$ are obtained by fitting $R_{eff}/\sin^2 \theta_e$ vs ω_e to eqs 19 and 22. The experimental dependence of $R_{eff}/\sin^2 \theta_e$ on ω_e is illustrated in Figure 6 for three residues in the fibronectin type III domain of the extra cellular matrix protein tenascin.[121] Intermediate time scale dynamics with $25 < \tau_{ex} < 100$ μs were observed for these residues.

Slow Time Scale Dynamics. If the chemical exchange time is slow, $\tau_{ex}\Delta\omega \gg 1$, then separate resonances are observed in the NMR spectrum for each conformation of the molecule. If, in addition, $\tau_{ex} \lesssim 1/R_1$, then exchange cross peaks are observable in homonuclear ^{1}H magnetization transfer (NOESY or ROESY) experiments, in heteronuclear longitudinal magnetization exchange spectroscopy, or in two-spin order exchange experiments.[109,122,123] The slow time scale regime extends approximately from milliseconds to seconds (for ^{1}H spins, $\tau_{ex}\Delta\omega = 3$ for $\tau_{ex} = 10^{-3}$ and $\Delta\omega = 1$ ppm). Heteronuclear longitudinal magnetization or two-spin order exchange experiments have the advantage of the increased resolution afforded by heteronuclear NMR spectroscopy; in addition, the autocorrelation peaks can be suppressed by difference spectroscopy.[123] The increased resolution of the heteronuclear longitudinal magnetization or two spin order exchange experiments is likely to make these experiments the methods of choice in future studies of slow exchange in biological macromolecules. For two-site exchange and spins lacking scalar couplings, the time dependence of the exchange peaks is given by (ignoring dipolar cross-relaxation)

$$\frac{d}{dt}\begin{bmatrix}\Delta M_{1z}(t)\\ \Delta M_{2z}(t)\end{bmatrix} = -\begin{bmatrix}R_{11} + k_1 & -k_{-1}\\ -k_1 & R_{21} + k_{-1}\end{bmatrix}\begin{bmatrix}\Delta M_{1z}(t)\\ \Delta M_{2z}(t)\end{bmatrix} \qquad (23)$$

in which $\Delta M_{1z}(t) = M_{1z}(t) - M_{1eq}$ and $\Delta M_{2z}(t) = M_{2z}(t) - M_{2eq}$ are the deviations of the magnetizations from equilibrium values at each site, and the system is assumed to be in microscopic equilibrium. If $R_{11} = R_{21} = \rho$ and $k_1 = k_{-1} = k$, then the time dependence of the diagonal and cross-peak volumes in an exchange spectrum are given by

$$\begin{aligned} I_{11}(t) = I_{22}(t) &= 0.5 \exp(-\rho t)[1 + \exp(-2kt)] \\ I_{12}(t) = I_{21}(t) &= 0.5 \exp(-\rho t)[1 - \exp(-2kt)] \end{aligned} \qquad (24)$$

The buildup of the exchange cross peak intensity is analyzed to determine the exchange rate constants. More complex kinetic schemes are analyzed using the formalism outlined for SSNMR (*vide infra*). The power of these experiments is illustrated by a study of the exchange between folded and unfolded forms of the drk SH3 domain.[109] Exchange rate constants for folding of 0.89 s^{-1} and R_1 for both folded and unfolded forms were determined simultaneously. An example of the exchange data is shown in Figure 7. Isomerization of the Cys 14 to Cys 38 disulfide bond in BPTI has been studied as a function of temperature over the range 277−341 K.[120] The observed temperature dependence of the exchange rates for ^{1}H−^{15}N two-spin order of Ala 16 from 277 to 293 K was used to determine an activation enthalpy of 13 ± 4 kcal/mol for isomerization; above 293 K, additional kinetic processes become evident.

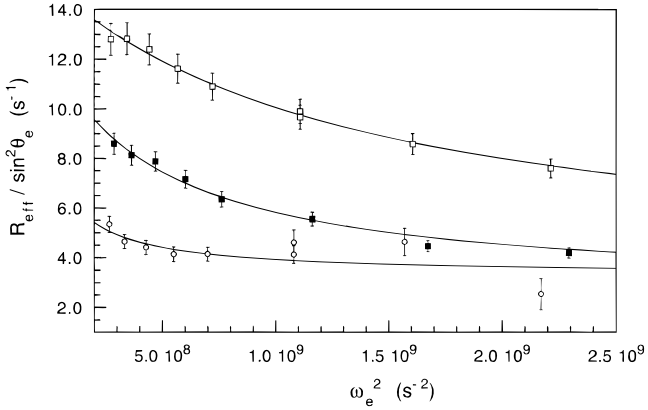

Figure 6. Intermediate time scale dynamics in the fibronectin type III domain of tenascin.[121] Representative relaxation dispersion curves for the backbone ^{15}N spins of (○) Asp 30, (■) Arg 45, and (□) Asn 55 obtained at eight different effective fields and a temperature of 300 K. The spin lock field strength was 2330 ± 30 Hz. The offsets from the center of the ^{15}N spectrum were 138, 115, 92, 69, 57, 46, 34, and 23 ppm. The solid curves show the best fit to eqs 19 and 22. For maximum precision, $R_2 - R_1$ was fixed at values calculated from R_1 and NOE measurements using the model-free formalism and a rotational correlation time of 4.4 ns. The optimized values of τ_{ex} and $p_1p_2(\Delta\omega)^2$ are as follows: Asp 30, 88 ± 68 μs and (61 ± 24) × 10^3 s^{-2}; Arg 45, 46 ± 5 μs and (2.15 ± 0.05) × 10^5 s^{-2}; Asn 55, 27 ± 2 μs and (4.5 ± 0.2) × 10^5 s^{-2}.

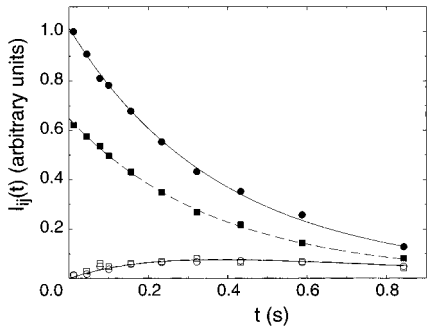

Figure 7. ^{15}N magnetization exchange data for Thr 12 of the drk SH3 domain.[109] $I_{ij}(t)$ is the integrated peak volume as a function of mixing time t. Solid symbols indicate data derived from the autocorrelation peaks for folded, $I_{11}(t)$, and unfolded protein, $I_{22}(t)$. Open symbols indicate data for the exchange cross peaks, $I_{12}(t)$ and $I_{21}(t)$. Data points marked with circles indicate magnetization originating in the folded state (species 1), and data points marked with squares indicate magnetization originating in the unfolded state (species 2). Lines are the fitted curves used to derive R_{11}, R_{12}, k_1, and k_{-1} by solution of eq 23.

An Example: Dihydrofolate Reductase. Dihydrofolate reductase (DHFR) is a small enzyme that has been the subject of intensive investigation by NMR spectroscopy and illustrates the applications of the above techniques. The backbone ^{15}N dynamics have been reported recently for the *E. coli* DHFR−folate binary complex.[124] Large-amplitude motions (low order parameters) on fast time scales were exhibited for a variety of sites in DHFR: residues in the adenosine binding site, hinge residues Lys 38 and Val 88, residues in βA−αB loop, and residues in the βF−βG loop. These regions are implicated in transition-state stabilization and ligand-dependent conformational changes. Significant $R_{ex} > 1$ s^{-1} were observed for 45% of the assigned resonances; the majority of these residues are clustered around the folate binding site and were suggested to reflect conformational exchange between distinct enzyme conformers of the binary complex. Slow exchange of Trp 42 in binding loop 1 was analyzed by ^{1}H magnetization exchange in NOESY spectra.[125] The results indicated that exchange between conformers occurs with a rate of 35 s^{-1}. DHFR illustrates a significant conclusion concerning dynamics of biological macromolecules: motional processes extending over time scales from picoseconds to seconds can contribute to function.

Solid State NMR Methods

The motivation to probe biopolymer dynamics by SSNMR has sometimes arisen due to the extreme insolubility of the molecule of interest or the fact that it would normally function in a solid-like state. In other instances, the interest has been due to the particular strengths and accuracy of solid-state methods. The desire to compare SSNMR results with X-ray crystallographic results for the same molecule or to compare with data concerning related crystalline small molecules has also sometimes been important. Whatever the motivation, patency of the sample is important. In vivo conditions involve macromolecular assemblies that are quite concentrated with water typically being a limiting component. In some respects, these conditions are similar those used for SSNMR experiments; many SSNMR studies have utilized well-hydrated materials and temperatures close to physiological conditions. In many experiments, in situ functional assays partly address the concern of integrity of the sample and authenticity of the dynamical properties. Very few studies have compared the conformational dynamics of monodispersed solutions of biopolymers and concentrated hydrated precipitates.

SSNMR experiments require many milligrams of specifically labeled material (i.e., a unique or at most a few labels per molecule), which is only possible for certain proteins. The experiments are technically demanding and require excellent probe performance; that is, the shortest possible pulse lengths, good filling factor, and good homogeneity for both B_0 and B_1. Ultimately, relaxation measurements as a function of applied field will be of interest as well.

SSNMR methods for probing motion invariably take advantage of the modulation of anisotropic resonance frequencies by molecular motion. The most elegant body of work concerns deuterium NMR measurements of static (nonspinning) samples.[126−128] Deuterium NMR has been a popular probe for local conformational dynamics because the spectrum is dominated by a single interaction, the anisotropic quadrupolar interaction (of order 200 kHz), which contributes an offset from the Larmor frequency given by

$$\omega - \omega_0 = (\pm\omega_Q/2)[(3\cos^2\beta_{lp} - 1) + (\eta\sin^2\beta_{lp}\cos(2\gamma_{lp}))] \quad (25)$$

where ω_0 is the Larmor frequency, $\omega_Q = (3/4)(e^2qQ/\hbar)$ and e^2qQ/h is the quadrupolar coupling constant or QCC in hertz (typically 160−180 kHz for C−D bonds[129] and 50−300 kHz for O−D or N−D bonds,[130,131] depending upon the hydrogen bonding characteristics), β_{lp} is the polar angle relating the unique quadrupolar axis (the bond vector) to the applied field, γ_{lp} is the azimuthal angle relating the quadrupolar principal axes to the laboratory frame, and $\eta = (V_{xx} - V_{yy})/V_{zz}$ is the asymmetry factor for the electric field gradient tensor, **V** (η is nearly 0 for uniaxial C−D bonds and 0.05−0.2 for electronically less symmetric systems). The two transitions at $\omega_0 \pm \omega_Q$ correspond to the two allowed NMR transitions for the three-level system. Other interactions for the deuteron, such as chemical shielding and dipolar coupling normally are quite modest (of order 1 kHz or less); significant simplification is obtained by ignoring these terms. For certain experiments (such as T_2 measurements with

long refocusing times) deuteron−deuteron, deuteron−nitrogen, or deuteron−proton dipolar couplings can create complications for deuterium spectroscopy.[132]

The strength of the quadrupolar interaction corresponds approximately to the largest spectral bandwidth that is possible for most instruments; in this respect the sensitivity to motion is good. The deuteron offers opportunities to probe dynamic processes on many time scales: slow motions, of order milliseconds to seconds, through exchange, hole-burning, and T_2 anisotropy spectra; intermediate time scale motions, of order microseconds, through quadrupolar echo line shape analysis; and faster motions, of order nanoseconds to picoseconds, through analysis of anisotropic T_{1Z} and T_{1Q} or Jeener Broekaert/spin alignment, which is most sensitive to the spectral density at the Larmor frequency, in the limit that the Redfield analysis is valid.

Many deuterium dynamics experiments have analogies in the spectroscopy of more commonly utilized spin-$^1/_2$ nuclei such as ^{13}C and ^{15}N. The anisotropy of the chemical shielding interaction is utilized, which is significantly smaller than that of the quadrupolar interaction, and the relative importance of dipolar couplings to attached protons sometimes makes the analysis less clean. If several anisotropic or time-dependent interactions are of similar order of magnitude, then interference effects between these terms (e.g., dipolar and CSA cross-correlation effects) can be substantial.

For the purpose of simulating spectra, the effect of orientation and motion upon $\tilde{H}_1$, the Hamiltonian for the anisotropic interaction, is conveniently expressed in terms of second rank spherical tensor notation for both spin, $\tilde{\mathbf{A}}_M^{(2)}$, and spatial, $\mathbf{T}_M^{(2)}$, components

$$\tilde{H}_1(t) = \sum_{M=-2}^{2} (-1)^M \tilde{\mathbf{A}}_M^{(2)} \mathbf{T}_M^{(2)}(t) \tag{26}$$

The bold characters indicate a tensor or matrix, while the tilde (∼) specifically refers to a tensor or matrix accounting for spin components. Each entry of $\tilde{\mathbf{A}}_M^{(2)}$ is proportional to a spin variable tensor: $\tilde{\mathbf{A}}_0^{(2)} = (1/\sqrt{6})(3\tilde{I}_z^2 - \tilde{I}\cdot\tilde{I})$; $\tilde{\mathbf{A}}_{\pm 1}^{(2)} = (1/2)(\tilde{I}_z\tilde{I}_\pm + \tilde{I}_\pm\tilde{I}_z)$; $\tilde{\mathbf{A}}_{\pm 2}^{(2)} = (1/2)(\tilde{I}_\pm^2)$. Expressions for the antisymmetric portions of the Hamiltonian are omitted here because they do not contribute to the deuteron Hamiltonian and contribute negligibly to any of the anisotropic Hamiltonians of interest; the isotropic component is omitted here but would be found in the analogous expression for chemical shielding. The orientation dependence of the spatial portion of the Hamiltonian $\mathbf{T}_M^{(2)}(t)$ is formally introduced with Wigner rotation matrices $\mathbf{D}_{NM}^{(2)}[\Omega_{lp}(t)]$ relating the (time independent) principal axis system tensor components $\mathbf{T}_N^{(2),p}$ to the (time dependent) laboratory frame components $\mathbf{T}_M^{(2),l}(t)$ using Euler angles α, β, and γ that are conventionally summarized as Ω.

$$\mathbf{T}_M^{(2),l}(t) = \sum_{N=-2}^{2} \mathbf{D}_{NM}^{(2)}[\Omega_{lp}(t)]\mathbf{T}_N^{(2),p} \tag{27}$$

In the principal axis system the spatial tensor components for the deuteron can be very conveniently expressed: $\mathbf{T}_0^{(2),p} = (\sqrt{3/8})(e^2qQ/\hbar)$; $\mathbf{T}_{\pm 1}^{(2),p} = 0$; $\mathbf{T}_{\pm 2}^{(2),p} = \eta e^2qQ/4\hbar$. Analogous expressions have been summarized for other interactions (dipolar, CSA, etc.).[128] Properties of the rotation matrices are summarized elsewhere.[128,133] These time-dependent rotation matrices, $\mathbf{D}_{NM}^{(2)}[\Omega_{lp}(t)]$, convey the essence of the motional model. For computational convenience, the time-dependent transformation from the principal axis system for each site to the laboratory frame is computed in two steps:

$$\mathbf{D}_{NM}^{(2)}[\Omega_{lp}(t)] = \sum_{F=-2}^{2} \mathbf{D}_{NF}^{(2)}[\Omega_{lc}]\mathbf{D}_{FM}^{(2)}[\Omega_{cp}(t)] \tag{28}$$

An analogous expression describes the time-independent relation between the principal axis system for the jth site in a N-site jump model and the laboratory frame:

$$\mathbf{D}_{NM}^{(2)}[\Omega_{lp}]^j = \sum_{F=-2}^{2} \mathbf{D}_{NF}^{(2)}[\Omega_{lc}]\mathbf{D}_{FM}^{(2)}[\Omega_{cp}]^j \tag{29}$$

where $\mathbf{D}_{NF}^{(2)}[\Omega_{lc}]$ is the rotation from the crystal fixed frame to the laboratory frame (LF) (which is varied to create the powder average), and $\mathbf{D}_{FM}^{(2)}[\Omega_{cp}]$ represents the rotation from the principal axis system (PAS) to the crystal fixed frame (CFF). When simulations of magic angle spinning (MAS) experiments are performed, it is useful to include three transformations: one rotation that relates the PAS to the CFF can subsume the effects of molecular motion, one that relates the CFF to the rotor fixed frame (RFF) would be used to construct a powder average, and a third that relates the RFF to the LF conveys the strictly periodic time dependence associated with MAS.

The fast and slow time scale motions that modulate the Hamiltonian have rather different effects; where possible it is convenient to separate the Hamiltonian for the anisotropic interaction into an average and a modulating component:

$$\tilde{H}_1^{\text{total}}(t) = \tilde{H}_1^{\text{ave}} + \tilde{H}_1^{\text{mod}}(t) \tag{30}$$

The static component describes evolution of coherences and is particularly important for calculating line shapes, while the fluctuating component describes the random perturbations and is used to describe relaxation processes. The time average of the Hamiltonian can be performed by averaging the spatial dependence on an appropriate time scale to produce $\overline{\mathbf{T}_M^{2,l}}$ (i.e., the time scale should be long compared with the inverse of the Larmor frequency). The components of the Hamiltonian are then

$$\tilde{H}_1^{\text{ave}} = \sum_{M=-2}^{2} (-1)^M \tilde{\mathbf{A}}_M^{(2)} \bar{\mathbf{T}}_M^{(2),l} \tag{31}$$

and

$$\tilde{H}_1^{\text{mod}}(t) = \sum_{M=-2}^{2} (-1)^M \tilde{\mathbf{A}}_M^{(2)} \{\mathbf{T}_M^{(2),l}(t) - \bar{\mathbf{T}}_M^{(2),l}\} \tag{32}$$

The frequencies ω^j for the jth site with a crystallite orientation described by Ω_{lc} would be derived using $\tilde{H}_1^{j,\text{ave}}$ as described in eqs 31 and 29 to yield

$$\omega(\Omega_{lc})^{j,\text{ave}} = \frac{1}{\hbar}\sum_{M=-2}^{2} (-1)^M \tilde{\mathbf{A}}_M^{(2)} \{\sum_{N=-2}^{2}\sum_{F=-2}^{2} \mathbf{D}_{NF}^{(2)}[\Omega_{lc}]\bar{\mathbf{D}}_{FM}^{(2)}[\Omega_{cp}{}^j]\mathbf{T}_N^{(2),p}\} \tag{33}$$

The dependence upon crystallite orientation Ω_{lc} is written

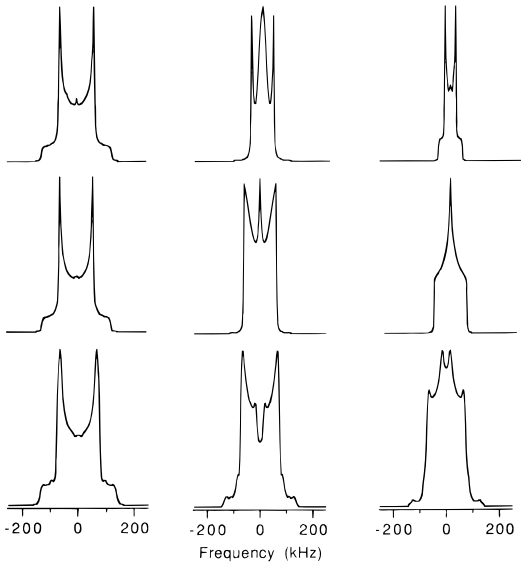

Figure 8. Simulations of quadrupolar echo spectra of a variety of motions. Top row assumes the three-site hopping motion of a methyl group; middle row assumes the trans−gauche isomerization as in a methylene chain; bottom row assumes the two-site flipping of a phenyl ring. Left column was computed assuming a rate of 10^4 s^{-1}; middle column was computed assuming a rate of 10^6 s^{-1}; right column was computed assuming a rate of 10^8 s^{-1}. The vertical scales are expanded by the following factors: (left to right of top row) 1, 5.6, 1.8; (left to right of middle row) 1.6, 2.5, 1.0; (left to right of bottom row) 1.5, 2.0, 1.0. The various models result in drastically different line shapes. Spectra were calculated with modified programs based upon those originally written and described by Wittebort, Olejniczak, and Griffin.[135]

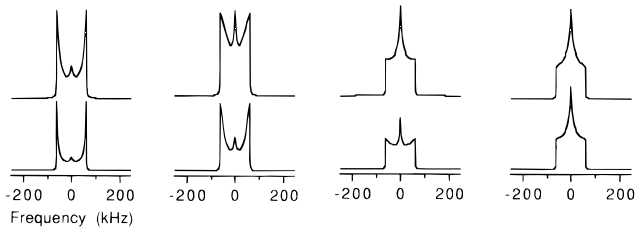

Figure 9. Simulation of τ-dependent spectra for a model of trans−gauche isomerization. Spectra simulated with the quadrupolar echo delay, τ, equal to 30 μs (top row) and 150 μs (bottom row); spectra were simulated using rates of 10^4, 10^5, 10^6, and 10^7 s^{-1} (left to right). The most dramatic effect occurs for relatively slower rates for which the inverse of the isomerization rate is comparable to the interpulse spacing.

explicitly to emphasize the anisotropic nature of the line shape and the powder averaging that is required for simulation. This expression is analogous to eq 25 but is more convenient for treating motion and orientational averaging.

Intermediate and Slow Time Scale Dynamics. When the molecule undergoes conformational exchange with a rate comparable to the anisotropic interaction, dramatic affects are seen in the line shape, analogous to the intermediate exchange processes seen in solution NMR. The use of anisotropic line shapes to analyze motions on the microsecond time scale is amply demonstrated through the spectra of simple amino acids. The type of motion (three-site hop of methyl groups, two-site flip of phenyl groups, etc.) has a pronounced effect on the features of the line shapes (Figure 8). Line shapes are detected using the τ-dependent quadrupolar echo pulse sequence ($90_x-\tau-90_y-\tau-$acquire) in order to refocus the magnetization for inhomogeneous and static systems. Variation of the temperature and refocusing delays produces dramatically different line shapes and altered intensities (Figure 9) that provide additional constraints for the proposed model. Please see the website (http://gibbs.chem.columbia.edu/~mcdhome/biopolymers) for more comprehensive series of motional models and associated line shapes. Figure 8 illustrates that the motional models can often be identified by qualitative inspection of the fast limit line shapes.

Comparisons of computed and experimental spectra (including τ-dependence and temperature dependence) can more quantitatively validate a proposed model and rule out incorrect models. The commutator $i[\tilde{\sigma}^j(t),\tilde{H}_1^{j,ave}]$, where $\tilde{\sigma}^j$ represents the density matrix for the jth site, is used to describe the time derivative or the evolution of coherences for the jth site in a N-site jump system. The resulting differential equation is presented here in a simplified form without the effects of relaxation *(vide infra)* and expressed for the complex transverse magnetization, for example M^j for the jth site[134,135]

$$\partial M(\Omega_{lc})^j/\partial t = \sum_{i=1}^{N}(i\omega(\Omega_{lc})^{ji} + k^{ji})M^i \qquad (34)$$

in which k^{ji} are entries in the matrix of rate constants for the conformational change, connecting sites i and j; to achieve detailed balance $k^{jj} = -\sum_{i=1}^{N} k^{ji}(1 - \delta_{ji})$. The frequencies are given by $\omega^{ij} = \omega^i\delta_{ij}$ where ω^i is derived using $\tilde{H}_1^{j,ave}$ as described in eq 33. The solution to this differential equation, assuming the use of a quadrupolar echo pulse sequence, is simply

$$M(t,\Omega_{lc}) = e^{(i\tilde{\omega}(\Omega_{lc})+\tilde{k})(t+\tau)}e^{-(i\tilde{\omega}(\Omega_{lc})+\tilde{k})\tau}M(0, \Omega_{lc}) \qquad (35)$$

$M(0, \Omega_{lc})$ represents the net z magnetization before the first pulse (typically the equilibrium magnetization). The transverse magnetization as a function of time, the free induction decay, is calculated by first diagonalizing the matrix $i\tilde{\omega} + \tilde{k}$, exponentiating the diagonal matrix and rotating the result back to the original frame of reference; Fourier transformation yields the spectrum. Details of the methods by which the diagonalizations are performed have been described.[134,135] The computation must be repeated for a random selection of crystallites and summed to construct the powder average.

Both two dimensional chemical exchange[136] and one-dimensional hole burning recovery[137−139] experiments have been developed that differentiate populations and other variables (rates and angles); stronger constraints on the motional model often result. These experiments are particularly important when low symmetry exists in the molecule so that equal populations should not be assumed; in this case separating the populations from other variables is essential for obtaining a reliable model of the motion. These experiments are sensitive to very slow time scales of motion, limited only by the spin−lattice relaxation.

Applications of line shape analyses to amino acids, and proteins up to 1986 have been reviewed.[4−6] These measurements have afforded accurate estimates of correlation times and activation energies for dynamics of amino acids in crystals and provide unambiguous evidence for tyrosine and phenylalanine ring flipping motions on the microsecond time scale and fast-limit ($\tau_c < 10^{-8}$ s) methyl group motions in alanine, valine, methionine, isoleucine, and leucine at room temperature. In nearly every case, the kinetic expression for activated processes provides a compact summary of the rates observed on these time scales. The extant literature differs somewhat as to whether significant activation entropies can be extracted, but for the most part the exponential prefactors are within an order of magnitude of that expected from the simple expression (kT/h). On the other hand, the asymmetric indole ring of tryptophan and the imidazole ring of histidine have *not* been observed to flip on

the microsecond or millisecond time scale; consequently, these groups serve as more sensitive probes of domain motions and larger scale rearrangements.

Most of the motions mentioned above concern nonexchangeable deuterons in groups that are predominantly hydrophobic. In addition, a substantial literature exists on the activated motions of hydrogen-bonded groups in small crystalline molecules that are quite relevant as model systems for the motions expected in proteins: water flipping,[140] amine rotation,[141,142] rotation of primary amides,[137,143] and detailed analysis of tautomerism in complex organic systems.[144−154] The analogous measurements in protein systems have been frustrated by the apparent impossibility of site-specific labeling.

Fast Time Scale Dynamics. When the rate of motion is much faster than the anisotropic frequency, "fast-limit" line shapes result, and further increases in the rate do not affect the line shape. In this regime, motion still has a pronounced effect upon relaxation rates. The most common SSNMR experiments for characterizing motions on a fast time scale are measurements of anisotropic relaxation. These experiments are most revealing if the rates of the motions are 10^7-10^{11} s^{-1} (of the same order as the deuterium Larmor frequency, typically 40−100 MHz) and the amplitudes of the motions are greater than about 20°. Deuterium spin−lattice relaxation is most commonly probed, but relaxation of other coherences is very useful as well. Deuterium spin−lattice relaxation measurements are performed with a simple nonselective 180° inversion pulse, followed by a variable relaxation delay and a quadrupolar echo detection. For a certain delay value, the "zero crossing", the integrated signal intensity is null, but the spectrum consists of positive and negative components and this pattern serves as a signature for the type of the molecular motion. Typically, in a T_1 anisotropy experiment, spectra are collected for a series of different time delays, centered about the "zero crossing". In favorable cases, temperature can be used to modulate the rate of the particular motion and thus provide a further constraint on the proposed model. Experimental data are interpreted by comparison with explicit simulations of the evolution of magnetization for various specific models of the motion. Anisotropic relaxation is often quite blatant: that is, various parts of the powder pattern recover at markedly different rates. Figure 10 illustrates computed "zero-crossing" T_1 anisotropy spectra for a three-site hop (methyl group and amine), trans−gauche isomerization (methylene chain such as a lysine), and the two-site flip (phenyl and tyrosine groups) at three different rates (10^6, 10^8, and 10^{10} Hz) of exchange between the sites; these simulations closely resemble experimental spectra for the corresponding functional groups.[65,126,155] A more comprehensive collection of simulations involving various rates and populations can be found at the website mentioned above. For fast motions the angle of the jump as well as the populations from the anisotropic recovery potentially can be recognized.

The relaxation rates are usually simulated using Redfield theory and an assumed motional model. The application of Redfield theory is valid only for fast and weak perturbations; $H_1(t)$ or, if appropriate, the modulated component of the Hamiltonian, $\tilde{H}_1^{\mathrm{mod}}(t)$ from eq 30, is used to compute transition rates. The rates must be separately calculated for each site involved in slow conformational exchange, as well as for each crystallite: a variety of properties that are discussed in the following, including the Redfield elements, the density matrices, the frequencies, the relaxation rates, and spectral densities are all explicit functions of orientation. Accordingly a superscript "j" as well as the crystallite orientation dependence Ω_{lc} should be included the following equations, but these instead are implicit for notational convenience. Typically, a powder spectrum is measured and simulated which means that the calculations should be performed for a random selection of crystallites and summed to produce the anisotropic and broad line.

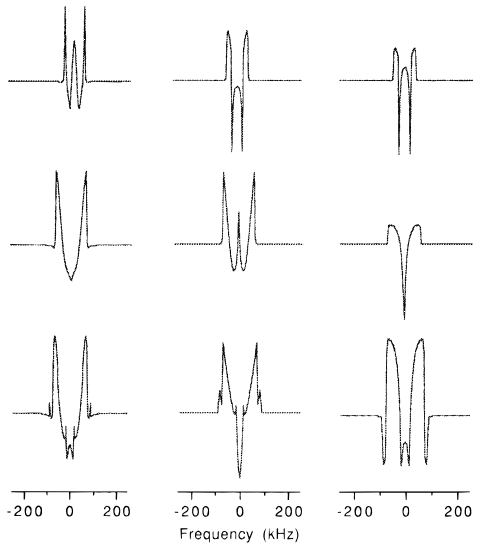

Figure 10. Simulations of quadrupolar echo detected T_{1Z} anisotropy near the zero crossing time. Top row assumes the three-site hopping motion of a methyl group. The quadrupolar coupling constant used was 167 kHz with $\eta = 0.0$; Euler angles = (0,109,0), (0,109,120), and (0,109,−120), populations = ($^1/_3$,$^1/_3$,$^1/_3$), and line broadening = 500 Hz. Middle row assumes the trans−gauche isomerization as in a methylene chain. The quadrupolar coupling constant used was 167 kHz with $\eta = 0.0$; Euler angles for each site = (0,109,0), (0,109,120); populations = ($^1/_2$,$^1/_2$); and line broadening = 500 Hz. Bottom row assumes the two-site flipping of a phenyl ring. The quadrupolar coupling constant used was 187 kHz with $\eta = 0.0$; Euler angles = (0,60,0) and (180,60,0) for deuterons δ and ϵ with populations ($^2/_5$,$^2/_5$); Euler angles = (0,0,0) for deuteron η with a population of ($^1/_5$); line broadening = 500 Hz. Left column was computed assuming a rate of 10^6 s^{-1}; middle column was computed assuming a rate of 10^8 s^{-1}; right column was computed assuming a rate of 10^{10} s^{-1}. The vertical scales are expanded by the following factors: (left to right of top row) 3740, 87, 36; (left to right of middle row) 1029, 76, 38; (left to right of bottom row) 930, 46, 22. The T_1 values for the parallel and perpendicular edges are as follows. Left to right of top row: $T_1(\|)$ = 397 ms, $T_1(\perp)$ = 535 ms; $T_1(\|)$ = 4.8 ms, $T_1(\perp)$ = 6.93 ms; $T_1(\|)$= 2.76 ms, $T_1(\perp)$ = 5.5 ms. Left to right of middle row: $T_1(\|)$ = 500 ms, $T_1(\perp)$ = 500 ms; $T_1(\|)$ =6.4 ms, $T_1(\perp)$ = 5.9 ms; $T_1(\|)$ = 137 ms, $T_1(\perp)$ = 69 ms. Left to right of bottom row: $T_1(\|)$ = 534 ms, $T_1(\perp)$ = 763 ms; $T_1(\|)$ = 27.8 ms, $T_1(\perp)$ = 40.3 ms; $T_1(\|)$ = 4.8 ms, $T_1(\perp)$ = 104 ms. The various models result in drastically different T_1 crossing spectra as well as T_1 values. Spectra were calculated with modified programs based upon those originally written and described by Wittebort, Olejniczak, and Griffin.[155] An extensive set of simulations that more fully covers the different parameters for various models has been deposited at http://gibbs.chem.columbia.edu/~mcdhome/biopolymers.

Relaxation matrix elements, R_{pqrs}, describe the total relaxation of the coherence σ_{pq} in relation to all other coherences as indicated by the expression:

$$\partial\sigma_{\mathrm{pq}}/\partial t = \mathrm{i}\omega_{qp}\sigma_{pq} + \sum_{rs} R_{pqrs}\sigma_{rs} \tag{36}$$

The relaxation elements are derived from individual transition rates using the well-known expressions:

$$R_{pqrs} = J_{prqs}(\omega_{sq}) + J_{prqs}(\omega_{pr}) - \delta_{qs}\sum_n J_{nrnp}(\omega_{np}) - \delta_{pr}\sum_n J_{nqns}(\omega_{qn}) \tag{37}$$

(in which δ_{ij} is the Kronecker delta). The elemental transition probabilities $J_{pqrs}(\omega)$ are given by

$$J_{pqrs}(\omega) = \int_0^\infty \langle p|\tilde{H}_1^{\text{mod}}(t)|q\rangle\langle r|\tilde{H}_1^{\text{mod}}(t+\tau)|s\rangle^* e^{-i\omega\tau}\, d\tau \quad (38)$$

and the rapidly modulated component of the Hamiltonian is given by

$$\tilde{H}_1^{\text{mod}}(t) = \sum_{M=-2}^{2} (-1)^M \tilde{A}_M^{(2)} \{\mathbf{T}_M^{(2),l}(t) - \overline{\mathbf{T}_M^{(2),l}}\} \quad (39)$$

where $\overline{\mathbf{T}_M^{2,l}}$ is the time average of $\mathbf{T}_M^{(2),l}(t)$. $H_1^{\text{mod}}(t)$ is assumed to be stationary, and all ensemble properties are then independent of t. Substitution of eq 39 into eq 38 yields

$$J_{pqrs}(\omega) = \sum_{M=-2}^{2} (-1)^M (T_0^{(2),p})^2 \langle p|\tilde{A}_M{}^2|q\rangle\langle r|\tilde{A}_M{}^2|s\rangle^* J_M(\omega) \quad (40)$$

The spectral density function, $J_M(\omega)$, and its Fourier transform, the correlation function $C_M(t)$, are defined by

$$J_M(\omega) = \int_0^\infty C_M(t)\cos(\omega t)\, dt \quad (41)$$

$$C_M(t) = \left(\frac{1}{T_0^{2,p}}\right)^2 \{\mathbf{T}_M^{(2),l}(0) - \overline{\mathbf{T}_M^{(2),l}}\}^* \{\mathbf{T}_M^{(2),l}(t) - \overline{\mathbf{T}_M^{(2),l}}\} \quad (42)$$

These quantities describe the motion and are normalized so that they are independent of the strength of the particular interaction and of the spin coordinates.

As an example, the spin−lattice relaxation rate of the spin-1 quadrupolar Hamiltonian, in the limit that the motion is rapid compared with the anisotropic interaction, is given by

$$R_{1Z} = \frac{1}{T_{1Z}} = R_{1122} + 2R_{1133} = 2J_{1212} + 4J_{1313} = \frac{3}{8}\left(\frac{e^2qQ}{\hbar}\right)^2 [J_1(\omega_0) + 4J_2(2\omega_0)] \quad (43)$$

The expression would be computed for each crystallite, and the resonance frequency for the crystallite would be separately evaluated, including the effects of conformational exchange as discussed above. The powder averaged anisotropic relaxation line shapes are calculated by adding together the contribution to a particular recovery time for each crystallite at the appropriate frequency. While an exponential process would result for each crystallite from this treatment, spectral components decay nonexponentially because numerous crystal orientations coincidentally achieve the same spectral frequency. For rigid uniaxial systems, the components at $\omega - \omega_0 = \pm(3/4)(e^2qQ/\hbar)$ or 0 are important exceptions because these frequencies correspond to unique crystal orientations, parallel to the field ($\theta = 0$) and at the "magic angle" relative to the field ($\theta = \cos^{-1}(1/\sqrt{3})$) according to eq 25.

Spin−lattice relaxation is by far the most common measurement that has been performed for biological solids, although analogous expressions for the relaxation of transverse magnetization, T_2, of quadrupolar order, T_{1Q}, and of double quantum coherences T_{1DQ}, and pulse sequences for performing these measurement have been discussed.[14,126,127,128] If all of these measurements are performed, then determination of $J(0)$, $J(\omega_0)$, and $J(2\omega_0)$ may be possible with some redundancy provided the motions are all in the fast limit; this is analogous to spectral density mapping as performed in solution NMR. Lamentably few examples of T_{1Z} and T_{1Q} anisotropy measurements have been reported for proteins. The spectral densities can then be related to motional models via simulations. Each motional model corresponds to only one spectral density function, but the experimental spectral density functions can in principle be compatible with many motional models especially when the spectral density is measured only at a few select frequencies. The absence of relaxation processes associated with overall hydrodynamic tumbling can make internal degrees of freedom prominent in solid-state NMR relaxation experiments. Despite this fact, several distinct models are often compatible with experimental relaxation data. Rather than explicitly simulating the spectra, the decay of unique spectral components can be plotted, and these relaxation constants can be interpreted to give correlation times, using an analytic form for the spectral density function derived from a previously determined motional model and a kinetic limit (slow or fast).[6]

Analytic expressions for the spectral densities have been solved for a variety of models: diffusion in a cone or on a surface of a cone (which have been very popular for interpretation of solution NMR data).[65,155] Modified Lipari−Szabo formalisms have been used to interpret (isotropic) relaxation associated with small angle fluctuations for solid state samples.[156,157] N-site jump models with arbitrary populations have been very commonly used for interpreting solid-state NMR spectra.[65,126,155] The popularity is associated with the fact that this approach is very general: its most natural applications is for the side chain motions of the amino acids, but this model has also been used to treat anisotropic librations by breaking the motion into many small angle steps. The expression for the spectral density for the N-site jump model, in terms of the jump angles $\mathbf{D}_{mn}^{(2)*}[\Omega_{cpj}]$ and the rate matrix $\mathbf{k}$, is solved by first diagonalizing $\mathbf{k}$,

$$\mathbf{k}\mathbf{X}^{(g)} = -\lambda_g \mathbf{X}^{(g)} \quad (44)$$

to obtain eigenvectors $\mathbf{X}^{(g)}$ and eigenvalues λ_g (with g taking values from 0 to $N-1$). The zeroth eigenvector (with eigenvalue 0) contains the populations of the sites. The other eigenvalues and eigenvectors embody the time dependence of the rotation matrices and give rise to the following expression for the spectral density:

$$J_M(\omega) = \sum_{a,a'=-2}^{2} d_{Ma}^{(2)}(\theta)\, d_{Ma'}^{(2)}(\theta) e^{i(a-a')\phi} \sum_{n,l,j=0}^{N-1} \int_0^\infty e^{-\lambda_n t} \times \cos(\omega t)\, dt\, X_1^{(0)} X_1^{(n)} X_j^{(0)} X_j^{(n)} d_{0a}^{(2)}(\Theta_1)\, d_{0a}^{(2)}(\Theta_j) e^{i(a\Phi l - a'\Phi j)} \quad (45)$$

where θ and ϕ describe the relation between the crystal fixed frame and the laboratory frame, and Θ_j and Φ_j (for site j) describe the relation between the crystal fixed frame and the principal axis system.

A general method for computing partially relaxed anisotropic deuterium spectra incorporates Redfield relaxation elements into an N-site jump model[62,125,154] utilizing the density matrix formalism and a direct extension of the stochastic Liouville equation to treat a discrete number (N) of deuterium sites (labeled i, j...) connected by rate constants (k^{ij}) describing chemical exchange. The chemical exchange or site-to-site hopping rates, in concert with the evolution of coherences under the influence of the average Hamiltonian, introduce line shape effects, while the matrix of spin−lattice relaxation rates ($\tilde{R}_1^j$) describe the effects of any fast-limit motions: both line shape and relaxation are implicitly included. This approach is

summarized in the following master equation and has been described in more detail in another review:[126]

$$\frac{\partial}{\partial t}\begin{pmatrix}\tilde{\sigma}^1\\ \tilde{\sigma}^2\\ \vdots\\ \tilde{\sigma}^N\end{pmatrix} = \begin{pmatrix} i\tilde{\tilde{\Omega}}^1 + \tilde{R}^1 + \tilde{k}^{11} & \cdots & \tilde{k}^{1N}\\ \vdots & \ddots & \\ \tilde{k}^{N1} & & i\tilde{\tilde{\Omega}}^N + \tilde{R}^N + \tilde{k}^{NN}\end{pmatrix}\begin{pmatrix}\tilde{\sigma}^1\\ \tilde{\sigma}^2\\ \dots\\ \tilde{\sigma}^N\end{pmatrix} \quad (46)$$

The superoperator $\tilde{\tilde{\Omega}}^j$ generates the commutator $i[\tilde{\sigma}^j(t), \tilde{H}^{j,\text{static}}]$ driving the evolution of coherences for the jth site. The relaxation rate matrix $\tilde{R}^j$ for the jth site has elements R_{pqrs} as indicated in eq 36 and is generated from the time-dependent portion of the Hamiltonian, $\tilde{H}_1^{\text{mod}}$ as discussed above. To compute the broad line shape that occurs for a random powder, this equation must be solved for a large number of randomly selected orientations of the crystallite.

Significant simplifications relative to the full treatment in eq 46 are possible via the following assumptions: the spin states do not change during the sudden conformational change; the rate of conformational change is independent of the spin state (i.e., the $\tilde{k}^{ij}$ are diagonal matrices equal to a rate k^{ij} times the identity matrix); spin evolution does not occur during the jump process; the quadrupolar coupling tensor is uniaxial. These approximations and others have been discussed.[65,126,155]

The use of anisotropic relaxation measurements in biophysics is best illustrated by detailed analyses of lipid systems in which fast limit motions are the rule rather than the exception.[8,158−161] The resulting motional models have been supported with T_{1Q} measurements in some cases. In several instances, the data can be adequately accommodated by a model including a small number of correlation times (typically describing trans−gauche isomerization and axial diffusion) and a temperature dependence corresponding to an activated process.

Librations of amides have been studied via line shapes and through anisotropic T_1 measurements[162] of simple polyamides that serve as model systems for rapid backbone motions in proteins[163] (Figure 11). The spectra unambiguously indicate that the low angle fluctuations of the amide plane in a polyamide are anisotropic, and the principal modulation is an out-of-plane motion of the deutreron. These studies also suggest that the effective time scale of the amide rocking motion (but not the amplitude) systematically varies with the structure of the amide. It is likely that the motion is not well described by a single correlation time. Several SSNMR other measurements of protein backbone dynamics, including both relaxation and line shape information, are described in the following.

For complex motions with broad distributions of conformational kinetic constants, the fast limit approximation cannot be justified and a full quantum mechanical treatment of the spin system and lattice using the stochastic Liouville equation (rather than simply using the Redfield expressions) may be required. In a thorough analysis, which amply highlights the strengths of anisotropic measurements in elucidation of fundamental properties of polymer thermal motions (Tse, Hoatson, Vold, and Brown unpublished[164]) have demonstrated that librational motions in polycarbonate are characterized by a very broad distribution of correlation times that is poorly approximated by a single exponential process. Taken together with the substantial body of work on non-Arrhenius behavior in heme proteins by optical methods, these studies raise the issue of whether biopolymer motions can be successfully decomposed with a Lipari−Szabo formalism. Although the possibility of broad distributions of correlation times has been discussed in the context of line shape analysis,[165] the implication of this motional model for NMR experiments, both in solution and solid states, merits additional attention.

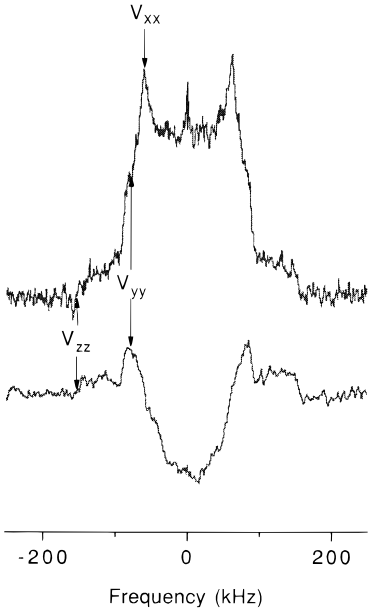

Figure 11. Anisotropic relaxation spectra of deuterium-exchanged lauryllactam measured at room temperature with a deuterium resonance frequency of 60.1 MHz. The data were collected with a nonselective inversion pulse followed a 0.7 s delay (just before the "zero crossing") and detected using a quadrupolar echo. The static like spectra indicates the absence of large-amplitude motions (cone angles greater than 20°). The partially relaxed spectrum shows that the *z*- and *y*-components relax faster than the *x*-component and suggests the presence of an out-of-plane libration.[162] The T_1 is 1.2 s at room temperature, indicating that this libration produces significant spectral density at frequencies comparable to the Larmor frequency (ω_0 and $2\omega_0$). The relaxation rates for a number of small crystalline amides was found to correlate with the dihedral angles adjacent to the amide.

Biological Applications. SSNMR line shape and relaxation measurements data are available for a handful of proteins: these include bacteriorhodopsin, collagen, fd phage viral coat protein, SNase, myoglobin, triose phosphate isomerase (TIM), and gramicidin. Often the studies incorporate both line shape and anisotropic relaxation data. Although nucleic acid research is not the focus of this review, it is worth noting that extensive analyses of local motions in hydrated double-stranded DNA also have been performed with site specific labeling in numerous locations, and measurements of both T_{1Z} and T_{1Q} and led to very interesting results concerning restriction enzyme binding motifs.[7,166−170]

Studies of the membrane proteins bacteriorhodopsin[171,172] and gramicidin have been reported; the main strength of these studies were line shape analysis (*vide infra*).[173,174] Carbon and deuterium NMR spectroscopy of bacteriorhodopsin[172,175,176] indicate that loops and termini are much more mobile than the membrane bound helical regions. Furthermore, internal sidechains often are more rigid than surface sidechains; aggregation of bacteriorhodopsin caused decreased mobility in the side chains.[132,177] The buried residues exhibit symmetric jump motions similar to those seen in crystalline amino acids, for example tyrosine and phenylalanine flips (on the millisecond

and microsecond time scales) and methyl rotations (on the nanosecond time scale). In principle, activation barriers for these motions can be extracted quantitatively. A study of site specifically deuterated retinal in bacteriorhodopsin illustrated the use of conformational dynamics (involving both line shape and relaxation analyses) in solving a structural question concerning the retinal conformation.[171] Studies of the fd viral coat protein contrasted the structural form and the membrane bound form; the latter showed significantly increased microsecond scale dynamics.[4,178] Recent studies on the backbone motions in gramicidin were based primarily on the reduction in apparent linewidth of ^{15}N powder patterns associated with changes in hydration and temperature. Angular fluctuations in the core of the channel were observed that are somewhat larger (up to 22°) than those seen in crystalline amides or typically seen in secondary structure elements of folded proteins (15−18°). A proposal for the relevance of these fluctuations to ion transport was presented.[173,174]

Motions in the active sites of a variety of enzymes have also been characterized by SSNMR. A detailed comparative study of the dynamical properties of SNase in the solution and solid states has also been reported recently.[156,157] SSNMR line shape and relaxation data were also used to probe the micro- and millisecond dynamics of a deuterated tryptophan residue in the catalytically essential flexible loop 6 of TIM[179] and led to the conclusion that motions consistent with the loop opening and closing seen in crystal structures could occur on the microsecond but not the nanosecond time scale. In both the presence or the absence of active site ligands, the ratio of the populations of the closed and open states is quite skewed. Anisotropic relaxation data have been reported for the case of a tryptophan in the flexible loop of TIM[179] but not yet quantitatively analyzed. Studies of the dynamics of bound substrate mimics by SSNMR have also been reported, the most recent of which concerns carboxy peptidase.[180]

^{13}C, ^{2}H, and ^{15}N relaxation measurements have been used in studying motions of backbones and sidechains in structural proteins such as keratin and collagen.[181−183] Characterization of the cytoskeletal protein keratin (intermediate epithelial filaments) by deuterium line shapes and anisotropic relaxation[181] showed differential flexibility in end domains and in the coiled coils; backbone, but not sidechain, groups of the coiled coils were significantly more rigid that those of the end domain. ^{2}H, ^{13}C, ^{19}F, and ^{15}N studies of collagen, including both line shape and relaxation measurements,[183] showed the side chain mobility, which involved angles of 11−30° at room temperature, to be independent of mineralization and dependent upon temperature. In contrast the backbone mobility on the low nanosecond time scale showed strong dependence upon both mineralization and temperature and was restricted to 5−10° even at room temperature. A model was presented in which the sidechain mobility of mineralized samples was related to the unusual mechanical properties of collagen.

Remaining Challenges for SSNMR. The motions of amino acids or other simple systems and those of protein domains are distinguished by the typical values for the populations of the sites undergoing kinetic interconversion. Symmetric motions in amino acids and other simple chemical solids are necessarily characterized by equal populations in a small number of sites that differ dramatically in their polar angle relative to a crystal fixed frame. In contrast, domain motions in proteins are characterized by populations that are highly skewed. In the case of the TIM loop, a 10:1 excess of the state visualized by diffraction methods was estimated to be in dynamic equilibrium with a second state (Figure 12). Naturally, as the population ratios become more skewed, the line shapes are more difficult to analyze, especially considering the typical signal-to-noise ratios that are achieved for biological solids. Techniques are needed to enhance the sensitivity of these measurements specifically for minor conformers. Hole burning recovery measurements have been applied to estimate the populations for the problem of loop flexibility.[179] Analogous information can be achieved with macroscopically ordered samples, as illustrated with elegant work on myoglobin.[177]

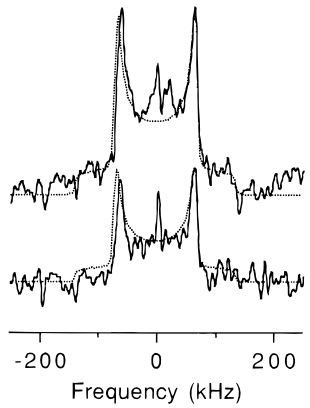

Figure 12. Quadrupolar echo spectra of deuterated tryptophan in loop 6 of TIM detected using 30 and 120 μs refocusing delays (the larger and smaller spectrum, respectively); measurements were performed at 5 °C on 50 mg of an active, hydrated enzyme precipitated using poly(ethylene glycol). The spectra shown were collected at 60.1 MHz with a recycle delay of 1 s. The number of scans for each spectrum is 20 000. Smooth simulated line shapes superimposed on the data were calculated assuming the angles derived from crystallographic measurements (pdb1ypi.ent for open state and pdb2ypi.ent for closed state[187,188]), a population ratio for the two sites of 1:10, and a jump rate of 3×10^4 s^{-1}.[179] Hole-burning recovery spectra (data not shown) indicated that one conformer is in excess over the other (ca. 8-fold); this observation was helpful in constraining the simulations and obtaining a jump rate for the loop. The anisotropic relaxation data (not shown) for the same sample indicated an out-of-plane libration with mean angles much smaller than those indicated by X-ray crystallography, although the direction of travel of the ring appears to be similar. The data indicate that opening and closing of the loop occurs at a rate comparable to enzymatic turnover.

In the future, more detailed methods for characterizing conformational dynamics of solids in a fashion consistent with high resolution SSNMR (e.g., MAS and proton decoupling) must be developed, in order to improve the sensitivity of the measurements and also to pursue possibilities for resolving and assigning several isotopically labeled sites. Both experimental approaches introduce additional perturbations to the Hamiltonian that must be treated explicitly.[184,185] The time evolution of deuterium magnetization under the influence of a periodic Hamiltonian associated with MAS and a random fluctuation associated with conformational dynamics has been computed using the stochastic Liouville equation and the Floquet formalism.[184] Even allowing for generous inhomogeneous broadening, pronounced effects in the line shape are associated with conformational dynamics over a very broad range of correlation times. In the intermediate regime, when the rates are comparable with the quadrupole splitting, severe broadening and loss of spinning sidebands are expected. An analogous effect is seen in the MAS spectra of ^{15}N or ^{13}C when the correlation time is comparable with the inverse of the decoupling Rabi frequency.[185] Theoretical simulations for these experiments are more complicated and the information garnered less robust in many cases than "static" measurements, but the improvement in efficiency associated with high-resolution measurements commands additional attention.

The opportunities for comparison of SSNMR measurements with other experimental probes and computational methods are substantial. Motions on the nanosecond and picosecond time scales can be conveniently compared with several other types of measurements, most notably solution NMR relaxation data and fluorescence spectroscopy. The use of molecular dynamics calculations to confirm the motions indicated by SSNMR anisotropic relaxation measurements is also very attractive although largely unexplored at the moment. On the millisecond time scale, chemical exchange methods in solution NMR are often available and rapid mix nonequilibrium methods (detected usually by optical techniques) are also possible. On the microsecond to millisecond time scale NMR data can be compared with phosphorescence or EPR, both of which require a molecular probe of modest dimensions. Solution NMR methods that probe these time scales, such as rotating frame relaxation measurements, are under development *(vide supra)* but might be applicable only for rather small proteins. In contrast to the situation for fast motions, where comparison with molecular dynamics simulations can be quite fruitful, simulations for these slower motions have not been prolific or successful. Simulations of databases of energetic barriers in terms of molecular modeling or *ab initio* methods have been attempted,[140,142] but quantitative agreement with experiment without use of bulk scaling factors still awaits further development; some of the problems appear to be associated with accounting for dielectric relaxation on slower time scales.

Perspectives for the Future: Solid State and Solution Studies

A particularly promising approach to studying dynamical properties of biological molecules combines solution and solid state NMR spectroscopy. Global analysis of molecular dynamics can be performed most easily by solution-state NMR; subsequently, interesting sites in the molecule thereby identified can be studied in greater detail by SSNMR spectroscopy.

An example of this approach is offered by SNase. An extensive study of SNase allowed comparison of dynamic properties in the solution[26,81] and solid states:[156,157,186] (1) Both solution and solid state investigations are consistent with SNase possessing a relatively rigid backbone. With the exception of the termini, most amides are relatively rigid on fast time scales with order parameters on the order of 0.86 in solution; the order parameters measured from solid state data were in the range 0.78−0.9, corresponding to a threefold variation in the ^{15}N R_1 values. (2) Exchange broadening of the Ω loop was observed in both solution and solid states. (3) Isotropic chemical shifts agreed well between the solution and solid states. (This observation has also been made for the case of myoglobin.[177]) (4) Considerable site-to-site variations in side chain flexibility were observed in both states. Solution studies indicate that the side chain flexibility is significantly reduced for the six leucines with a C^{δ} atom within 10 Å of the Ca^{2+} or a heavy atom of the thymidine 3′,5′-bisphosphate ligands. (5) A correlation between the backbone ^{15}N relaxation in the crystalline state and the *B* factors determined by X-ray crystallography was reported. Low correlation was observed for solution order parameters and *B* factors.

Application of the full range of solution and solid-state NMR techniques for studying molecular dynamics has yet to be accomplished for any macromolecule; by implication in no system have the insights potentially available from NMR spectroscopy been exhausted. Assessing the role of conformational dynamics in determining the physical and biological properties of biopolymers is a problem of long-standing importance that requires experimental and theoretical contributions from physical and biological perspectives. The relentless advance in experimental NMR techniques over the past few years, that will doubtless continue for the foreseeable future, will render detailed comparative studies of macromolecular dynamics in solid state and solution ever more enlightening.

Acknowledgment. We thank Mikael Akke, Arthur Mandel, and Tatyana Polenova for careful reading of the manuscript and helpful discussions. We thank Neil Farrow, Lewis E. Kay, Jeff Peng, and Gerhard Wagner for providing figures describing their work; we also thank Daiwen Yang and Lewis E. Kay for providing a preprint of ref 92. A.M. thanks the Research Corporation of America for financial support through the Cottrell Scholar Program, the NIH for support (GM49964), and acknowledges support from the Kanagawa Academy of Science and Technology. J.W. acknowledges support from the von Humboldt Foundation. A.G.P. acknowledges support from the National Science Foundation, the Beckman Young Investigator Program, NIH (GM5029), and NSF (MCB9419049). Additional figures and supporting material associated with this review are available through the World Wide Web at http://gibbs.chem.columbia.edu/∼mcdhome/biopolymers.

References and Notes

(1) Jardetzky, O.; Lefevre, J.-F. *FEBS Lett.* **1994**, *338*, 246−250.
(2) Palmer, A. G. *Curr. Opin. Biotechnol.* **1993**, *4*, 385−391.
(3) Wagner, G. *Curr. Opin. Struct. Biol.* **1993**, *3*, 748−753.
(4) Opella, S. J. *Methods Enzymol.* **1986**, *131*, 327−361.
(5) Torchia, D. A. *Annu. Rev. Biophys. Bioeng.* **1984**, *13*, 125−144.
(6) Keniry, M. A.; Smith, R. L.; Gutowsky, H. S.; Oldfield, E. In *Structure and Dynamics: Nucleic Acids and Proteins*; Clementi, E., Sarma, R. H., Eds.; Adenine Press: New York, 1983; pp 435−449.
(7) Wang, A. C.; Kennedy, M. A.; Reid, B. R.; Drobny, G. P. *J. Magn. Reson., Ser. B* **1994**, *105*, 1−10.
(8) Griffin, R. G. *Methods Enzymol.* **1981**, *72*, 108−174.
(9) Rendell, R. W.; Ngai, K. L. A Fundamental Relation Between Microscopic and Macroscopic Relaxation Times: Evidence in Relaxation Data, National Technical Information Service, U.S. Department of Commerce, 1985.
(10) Glöckle, W. G.; Nonnenmacher, T. F. *Biophys. J.* **1995**, *68*, 46−53.
(11) Frauenfelder, H. *Annu. Rev. Biophys. Biophys. Chem.* **1988**, *17*, 451−479.
(12) Iben, I. E. T.; Braunstein, D.; Doster, W.; Frauenfelder, H.; Hong, M. K.; Johnson, J. B.; Luck, S.; Ormos, P.; Schulte, A.; Steinbach, P. J.; Xie, A. H.; Young, R. D. *Phys. Rev. Lett.* **1989**, *62*, 1916−1919.
(13) Redfield, A. G. *Adv. Magn. Reson.* **1965**, *1*, 1−32.
(14) Vold, R. L.; Vold, R. R. *Prog. NMR Spectrosc.* **1978**, *12*, 79−133.
(15) Freeman, R.; Witthkoek, S.; Ernst, R. R. *J. Chem. Phys.* **1970**, *52*, 1529−1544.
(16) Jeener, J.; Vlassenbroek, A.; Broekaert, P. *J. Chem. Phys.* **1995**, *103*, 1309−1332.
(17) Klimasauskas, S.; Kumar, S.; Roberts, R. J.; Cheng, X. *Cell* **1994**, *76*, 357−369.
(18) Borer, P. N.; LaPlante, S. R.; Kumar, A.; Zanatta, N.; Martin, A.; Hakkinen, A.; Levy, G. C. *Biochemistry* **1994**, *33*, 2441−2450.
(19) Eimer, W.; Williamson, J. R.; Boxer, S. G.; Pecora, R. *Biochemistry* **1990,** *29*, 799−811.
(20) Williamson, J. R.; Boxer, S. G. *Biochemistry* **1989**, *28*, 2819−2831.
(21) Xi, Z.; King, G. C. In *35th Experimental Nuclear Magnetic Resonance Conference*; Pacific Grove, CA, 1994; P81.
(22) Doddrell, D. M.; Pegg, D. T.; Bendall, M. R. *J. Magn. Reson.* **1982**, *48*, 323−327.
(23) Burum, D. P.; Ernst, R. R. *J. Magn. Reson.* **1980**, *39*, 163−168.
(24) Morris, G. A.; Freeman, R. *J. Am. Chem. Soc.* **1979**, *101*, 760−762.
(25) Kay, L. E.; Bull, T. E.; Nicholson, L. K.; Griesinger, C.; Schwalbe, H.; Bax, A.; Torchia, D. A. *J. Magn. Reson.* **1992**, *100*, 538−558.
(26) Kay, L. E.; Torchia, D. A.; Bax, A. *Biochemistry* **1989**, *28*, 8972−8979.
(27) Bax, A.; Sparks, S. W.; Torchia, D. A. *Methods Enzymol.* **1989**, *176*, 134−150.
(28) Skelton, N. J.; Palmer, A. G.; Akke, M.; Kördel, J.; Rance, M.; Chazin, W. J. *J. Magn. Reson., Ser. B* **1993**, *102*, 253−264.

(29) Bodenhausen, G.; Ernst, R. R. *J. Am. Chem. Soc.* **1982**, *104*, 1304−1309.
(30) Kay, L. E.; Prestegard, J. H. *J. Magn. Reson.* **1988**, *77*, 599−605.
(31) Mandel, A. M.; Palmer, A. G. *J. Magn. Reson., Ser. A* **1994**, *110*, 62−72.
(32) Palmer, A. G.; Cavanagh, J.; Wright, P. E.; Rance, M. *J. Magn. Reson.* **1991**, *93*, 151−170.
(33) Kay, L. E.; Keifer, P.; Saarinen, T. *J. Am. Chem. Soc.* **1992**, *114*, 10663−10665.
(34) Boyd, J.; Hommel, U.; Campbell, I. D. *Chem. Phys. Lett.* **1990**, *175*, 477−482.
(35) Kay, L. E.; Nicholson, L. K.; Delaglio, F.; Bax, A.; Torchia, D. A. *J. Magn. Reson.* **1992**, *97*, 359−375.
(36) Palmer, A. G.; Skelton, N. J.; Chazin, W. J.; Wright, P. E.; Rance, M. *Mol. Phys.* **1992**, *75*, 699−711.
(37) Muhandiram, D. R.; Yamazaki, T.; Sykes, B. D.; Kay, L. E. *J. Am. Chem. Soc.* **1995**, *117*, 11536−11544.
(38) Yang, D.; Kay, L. E. *J. Magn. Reson., Ser. B* **1996**, *110*, 213−218.
(39) London, R. E. In *Magnetic Resonance in Biology*; Cohen, J. S., Ed.; Wiley: New York, 1980; Vol. 1, pp 1−69.
(40) Clore, G. M.; Driscoll, P. C.; Wingfield, P. T.; Gronenborn, A. M. *Biochemistry* **1990**, *29*, 7387−7401.
(41) Vold, R. L.; Waugh, J. S.; Klein, M. P.; Phelps, D. E. *J. Chem. Phys.* **1968**, *48*, 3831−3832.
(42) Carr, H. Y.; Purcell, E. M. *Phys. Rev.* **1954**, *94*, 630−638.
(43) Meiboom, S.; Gill, D. *Rev. Sci. Instrum.* **1958**, *29*, 688−691.
(44) Noggle, J. H.; Shirmer, R. E. *The Nuclear Overhauser Effect: Chemical Applications*; Academic Press: New York, 1971; p 259.
(45) Peng, J. W.; Thanabal, V.; Wagner, G. *J. Magn. Reson.* **1991**, *94*, 82−100.
(46) Peng, J. W.; Wagner, G. *J. Magn. Reson.* **1992**, *98*, 308−332.
(47) Peng, J. W.; Wagner, G. *Biochemistry* **1995**, *34*, 16733−16752.
(48) Kördel, J.; Skelton, N. J.; Akke, M.; Palmer, A. G.; Chazin, W. J. *Biochemistry* **1992**, *31*, 4856−4866.
(49) Farrow, N. A.; Muhandiram, R.; Singer, A. U.; Pascal, S. M.; Kay, C. M.; Gish, G.; Shoelson, S. E.; Pawson, T.; Forman-Kay, J. D.; Kay, L. E. *Biochemistry* **1994**, *33*, 5984−6003.
(50) Boyd, J. *J. Magn. Reson., Ser. B* **1995**, *107*, 279−285.
(51) Nirmala, N. R.; Wagner, G. *J. Am. Chem. Soc.* **1988**, *110*, 7557−7558.
(52) Nirmala, N. R.; Wagner, G. *J. Magn. Reson.* **1989**, *82*, 659−661.
(53) Palmer, A. G.; Rance, M.; Wright, P. E. *J. Am. Chem. Soc.* **1991**, *113*, 4371−4380.
(54) Wand, A. J.; Bieber, R. J.; Urbauer, J. L.; McEvoy, R. P.; Gan, Z. *J. Magn. Reson., Ser. B* **1995**, *108*, 173−175.
(55) Yamazaki, T.; Muhandiram, R.; Kay, L. E. *J. Am. Chem. Soc.* **1994**, *116*, 8266−8278.
(56) Engelke, J.; Rüterjans, H. *J. Biomol. NMR* **1995**, *5*, 173−182.
(57) Dayie, K. T.; Wagner, G. *J. Magn. Reson., Ser. B* **1995**, *109*, 105−108.
(58) Kushlan, D. M.; LeMaster, D. M. *J. Am. Chem. Soc.* **1993**, *115*, 11026−11027.
(59) Palmer, A. G.; Wright, P. E.; Rance, M. *Chem. Phys. Lett.* **1991**, *185*, 41−46.
(60) Schweitzer, B. I.; Gardner, K. H.; Tucker-Kellogg, G. *J. Biomol. NMR* **1995**, *6*, 180−188.
(61) Li, Y.-C.; Montelione, G. T. *J. Magn. Reson., Ser. B* **1993**, *101*, 315−319.
(62) Li, Y.-C.; Montelione, G. T. *J. Magn. Reson., Ser. B* **1994**, *105*, 45−51.
(63) Grzesiek, S.; Bax, A. *J. Am. Chem. Soc.* **1993**, *115*, 12593−12594.
(64) Abragam, A. *Principles of Nuclear Magnetism*; Clarendon Press: Oxford, 1961; p 599.
(65) Wittebort, R. J.; Szabo, A. *J. Chem. Phys* **1978**, *69*, 1722−1736.
(66) Hertz, H. G. *Prog. NMR Spectrosc.* **1983**, *16*, 115−162.
(67) Lipari, G.; Szabo, A. *J. Am. Chem. Soc.* **1982**, *104*, 4546−4559.
(68) Lipari, G.; Szabo, A. *J. Am. Chem. Soc.* **1982**, *104*, 4559−4570.
(69) Clore, G. M.; Szabo, A.; Bax, A.; Kay, L. E.; Driscoll, P. C.; Gronenborn, A. M. *J. Am. Chem. Soc.* **1990**, *112*, 4989−4991.
(70) Brüschweiler, R.; Case, D. A. *Phys. Rev. Lett.* **1994**, *72*, 940−943.
(71) Farrow, N. A.; Zhang, O.; Szabo, A.; Torchia, D. A.; Kay, L. E. *J. Biomol. NMR* **1995**, *6*, 153−162.
(72) Ishima, R.; Nagayama, K. *J. Magn. Reson., Ser. B* **1995**, *108*, 73−76.
(73) Halle, B.; Wennerström, H. *J. Chem. Phys.* **1981**, *75*, 1928−1943.
(74) Stone, M. J.; Fairbrother, W. J.; Palmer, A. G.; Reizer, J.; Saier, M. H.; Wright, P. E. *Biochemistry* **1992**, *31*, 4394−4406.
(75) Mandel, A. M.; Akke, M.; Palmer, A. G. *J. Mol. Biol.* **1995**, *246*, 144−163.
(76) Schurr, J. M.; Babcock, H. P.; Fujimoto, B. S. *J. Magn. Reson., Ser. B* **1994**, *105*, 211−224.
(77) Mandel, A. M.; Akke, M.; Palmer, A. G. *Biochemistry*, submitted.
(78) Buck, M.; Boyd, J.; Redfield, C.; MacKenzie, D. A.; Jeenes, D. J.; Archer, D. B.; Dobson, C. M. *Biochemistry* **1995**, *34*, 4041−4055.
(79) Palmer, A. G.; Hochstrasser, R. A.; Millar, D. P.; Rance, M.; Wright, P. E. *J. Am. Chem. Soc.* **1993**, *115*, 6333−6345.
(80) Pascal, S. M.; Yamazaki, T.; Singer, A. U.; Kay, L. E.; Forman-Kay, J. D. *Biochemistry* **1995**, *34*, 11353−11362.
(81) Nicholson, L. K.; Kay, L. E.; Baldisseri, D. M.; Arango, J.; Young, P. E.; Bay, A.; Torchia, D. A. *Biochemistry* **1992**, *31*, 5253−5263.
(82) Kay, L. E.; Muhandiram, D. R.; Farrow, N. A.; Aubin, Y.; Forman-Kay, J. D. *Biochemistry* **1996**, *35*, 361−368.
(83) Berglund, H.; Baumann, H.; Knapp, S.; Ladenstein, R.; Härd, T. *J. Am. Chem. Soc.* **1995**, *1995*, 12883−12884.
(84) Brüschweiler, R.; Wright, P. E. *J. Am. Chem. Soc.* **1994**, *116*, 8426−8427.
(85) Woessner, D. E. *J. Chem. Phys.* **1962**, *36*, 1−4.
(86) Akke, M.; Skelton, N. J.; Kördel, J.; Palmer, A. G.; Chazin, W. J. *Biochemistry* **1993**, *32*, 9832−9844.
(87) Cheng, J.-W.; Lepre, C. A.; Chambers, S. P.; Fulghum, J. R.; Thomson, J. A.; Moore, J. M. *Biochemistry* **1993**, *32*, 9000−9010.
(88) Cheng, J.-W.; Lepre, C. A.; Moore, J. M. *Biochemistry* **1994**, *33*, 4093−4100.
(89) Fushman, D.; Weisemann, R.; Thüring, H.; Rüterjans, H. *J. Biomol. NMR* **1994**, *4*, 61−78.
(90) Nicholson, L. K.; Yamazaki, T.; Torchia, D. A.; Grzesiek, S.; Bax, A.; Stahl, S. J.; Kaufman, J. D.; Wingfield, P. T.; Lam, P. Y. S.; Jadhav, P. K.; Hodge, C. N.; Domaille, P. J.; Chang, C.-H. *Nature Struct. Biol.* **1995**, *2*, 274−279.
(91) Akke, M.; Brüschweiler, R.; Palmer, A. G. *J. Am. Chem. Soc.* **1993**, *115*, 9832−9833.
(92) Yang, D.; Kay, L. E. *J. Am. Chem. Soc.*, submitted.
(93) Mackay, J. P.; Shaw, G. L.; King, G. F. *Biochemistry* **1996**, *35*, 4867−4877.
(94) Zheng, Z.; Czaplicki, J.; Jardetzky, O. *Biochemistry* **1995**, *34*, 5212−5223.
(95) Tjandra, N.; Feller, S. E.; Pastor, R. W.; Bax, A. *J. Am. Chem. Soc.* **1995**, *117*, 12562−12566.
(96) Woessner, D. E. *J. Chem. Phys.* **1962**, *37*, 647−654.
(97) Brüschweiler, R.; Liao, X.; Wright, P. E. *Science (Washington, D.C.)* **1995**, *268*, 886−889.
(98) Barbato, G.; Ikura, M.; Kay, L. E.; Pastor, R. W.; Bax, A. *Biochemistry* **1992**, *31*, 5269−5278.
(99) Eriksson, M. A. L.; Berglund, H.; Härd, T.; Nilsson, L. *Proteins: Struct. Funct. Genet.* **1993**, *17*, 375−390.
(100) Palmer, A. G.; Case, D. A. *J. Am. Chem. Soc.* **1992**, *114*, 9059−9067.
(101) Chandrasekhar, I.; Clore, G. M.; Szabo, A.; Gronenborn, A. M.; Brooks, B. R. *J. Mol. Biol.* **1992**, *226*, 239−250.
(102) Ahlström, P.; Teleman, O.; Kördel, J.; Forsén, S.; Jönsson, B. *Biochemistry* **1989**, *28*, 3205−3211.
(103) Smith, P. E.; van Schaik, R. C.; Szyperski, T.; Wüthrich, K.; van Gunsteren, W. F. *J. Mol. Biol.* **1995**, *246*, 356−365.
(104) Brüschweiler, R. *J. Am. Chem. Soc.* **1992**, *114*, 5341−5344.
(105) Robinson, B. H.; Drobny, G. P. *Annu. Rev. Biophys. Biomol. Struct.* **1995**, *24*, 523−549.
(106) Peng, J. W.; Wagner, G. *Biochemistry* **1992**, *31*, 8571−8586.
(107) Ishima, R.; Nagayama, K. *Biochemistry* **1995**, *34*, 3162−3171.
(108) van Mierlo, C. P. M.; Darby, N. J.; Keeler, J.; Neuhaus, D.; Creighton, T. E. *J. Mol. Biol.* **1993**, *229*, 1125−1146.
(109) Farrow, N. A.; Zhang, O.; Forman-Kay, J. D.; Kay, L. E. *J. Biomol. NMR* **1994**, *4*, 727−734.
(110) Frank, M. K.; Clore, G. M.; Gronenborn, A. M. *Protein Sci.* **1995**, *4*, 2605−2615.
(111) Alexandrescu, A. T.; Evans, P. A.; Pitkeathly, M.; Baum, J.; Dobson, C. M. *Biochemistry* **1993**, *32*, 1707−1718.
(112) Alexandrescu, A. T.; Shortle, D. *J. Mol. Biol.* **1994**, *242*, 527−546.
(113) Shaw, G. L.; Davis, B.; Keeler, J.; Fersht, A. R. *Biochemistry* **1995**, *34*, 2225−2233.
(114) Orekhov, V. Y.; Pervushin, K. V.; Arseniev, A. S. *Eur. J. Biochem.* **1994**, *219*, 887−896.
(115) Deverell, C.; Morgan, R. E.; Strange, J. H. *Mol. Phys.* **1970**, *18*, 553−559.
(116) Wennerström, H. *Mol. Phys.* **1972**, *24*, 69−80.
(117) Allerhand, A.; Thiele, E. *J. Chem. Phys.* **1966**, *45*, 902−916.
(118) Tjandra, N.; Kuboniwa, H.; Ren, H.; Bax, A. *Eur. J. Biochem.* **1995**, *230*, 1014−1024.
(119) Szyperski, T.; Luginbühl, P.; Otting, G.; Güntert, P.; Wüthrich, K. *J. Biomol. NMR* **1993**, *3*, 151−164.
(120) Otting, G.; Liepinsh, E.; Wüthrich, K. *Biochemistry* **1993**, *32*, 3571−3582.
(121) Akke, M.; Palmer, A. G. *J. Am. Chem. Soc.* **1996**, *118*, 911−912.
(122) Montelione, G. T.; Wagner, G. *J. Am. Chem. Soc.* **1989**, *111*, 3096−3098.

(123) Wider, G.; Neri, D.; K. Wüthrich *J. Biomol. NMR* **1991**, *1*, 93−98.
(124) Epstein, D. M.; Benkovic, S. J.; Wright, P. E. *Biochemistry* **1995**, *34*, 11037−11048.
(125) Falzone, C. J.; Wright, P. E.; Benkovic, S. J. *Biochemistry* **1991**, *30*, 2184−2191.
(126) Vold, R. R.; Vold, R. L. *Adv. Magn. Opt. Reson.* **1991**, *16*, 85−171.
(127) Hoatson, G. L.; Vold, R. L. *NMR: Basic Princ. Prog.* **1994**, *32*, 1−67.
(128) Spiess, H. W. *NMR: Basic Princ. Prog.* **1980**, *15*, 59−213. Spiess, H. W. *J. Chem. Phys.* **1980**, *72*, 6755−6762.
(129) Jackisch, M. A.; Jarrett, W. L.; Guo, K.; Fronczek, F. R.; Butler, L. G. *J. Am. Chem. Soc.* **1988**, *110*, 343−347.
(130) Berglund, B.; Vaughan, R. W. *J. Chem. Phys.* **1980**, *73*, 2037−2043.
(131) Hunt, M. J.; Mackay, A. L. *J. Magn. Reson.* **1974**, *15*, 402−414.
(132) Baianu, I. C.; Gutowsky, H. S.; Oldfield, E. *Biochemistry* **1984**, *23*, 3105−3110.
(133) Brink, D. M.; Satchler, G. R. *Angular Momentum*; Clarendon Press: Oxford, 1968.
(134) Greenfield, M. S.; Ronemus, A. D.; Vold, R. L.; Vold, R. R.; Ellis, P. D.; Raidy, T. E. *J. Magn. Reson.* **1987**, *72*, 89−107.
(135) Wittebort, R. J.; Olejniczak, E. T.; Griffin, R. G. *J. Chem. Phys.* **1987**, *86*, 5411−5420.
(136) Schmidt, C.; Blumich, B.; Spiess, H. W. *J. Magn. Reson.* **1988**, *79*, 269−290.
(137) Williams, J. C.; McDermott, A. E. *J. Phys. Chem.* **1993**, *97*, 12393−12398.
(138) Brown, M. J.; Hoatson, G. L.; Vold, R. L. In *34th Experimental Nuclear Magnetic Resonance Conference*; St. Louis, MO, 1992; p P127.
(139) Lin, T. H.; Vold, R. R. *J. Phys. Chem.* **1991**, *95*, 9032−9034.
(140) Larsson, K.; Tegenfeldt, J.; Hermansson, K. *J. Chem. Soc., Faraday Trans.* **1991**, *87*, 1193−1200.
(141) Andrew, E. R. *Polymer* **1984**, *26*, 190−193.
(142) Gu, Z.; Ebisawa, K.; McDermott, A. *Solid State NMR*, accepted for publication.
(143) Heaton, N. J., Vold, R. L.; Vold, R. R. *J. Am. Chem. Soc.* **1989**, *111*, 3211−3217.
(144) Braun, J.; Schlabach, M.; Wehrle, B.; Kocher, M.; Vogel, E.; Limbach, H.-H. *J. Am. Chem. Soc.* **1994**, *116*, 6593−6604.
(145) Hoelger, C. G.; Limbach, H.-H. *J. Phys. Chem.* **1994**, *98*, 11803−11810.
(146) Golubev, N. S.; Smirnov, S. N.; Gindin, V. A.; Denisov, G. S.; Benedict, H.; Limbach, H.-H. *J. Am. Chem. Soc.* **1994**, *116*, 12055−12056.
(147) Scherer, G.; Limbach, H.-H. *J. Am. Chem. Soc.* **1994**, *116*, 1230−1239.
(148) Schlabach, M.; Scherer, G.; Limbach, H.-H. *J. Am. Chem. Soc.* **1991**, *113*, 3550−3558.
(149) Schlabach, M.; Rumpel, H.; Limbach, H.-H. *Angew. Chem., Int. Ed. Engl.* **1989**, *28*, 76−79.
(150) Schlabach, M.; Limbach, H.-H.; Bunnenberg, E.; Shu, A. Y. L.; Tolf, B.-R.; Djerassi, C. *J. Am. Chem. Soc.* **1993**, *115*, 4554−4565.
(151) Meschede, L.; Limbach, H.-H. *J. Phys. Chem.* **1991**, *95*, 10267−10280.
(152) Limbach, H.-H. *NMR: Basic Princ. Prog.* **1990**, *23*, 63−164.
(153) Usha, M. G.; Wittebort, R. J. *J. Am. Chem. Soc.* **1992**, *114*, 1541−1548.
(154) Wittebort, R. J.; Usha, M. G.; Ruben, D. J. *J. Am. Chem. Soc.* **1988**, *110*, 5668−5671.
(155) Torchia, D. A.; Szabo, A. *J. Magn. Reson.* **1982**, *49*, 107−121.
(156) Sparks, S. W.; Cole, H. B. R.; Torchia, D. A.; Young, P. E. *Chem. Scr.* **1989**, *29A*, 31−38.
(157) Cole, H. B. R.; Torchia, D. A. *Chem. Phys.* **1991**, *158*, 271−281.
(158) Speyer, J. B.; Weber, R. T.; Gupta, S. K. D.; Griffin, R. G. *Biochemistry* **1989**, *28*, 9569−9574.
(159) Seelig, J. *Q. Rev. Biophys.* **1977**, *10*, 353−418.
(160) Jarrell, H.; Smith, I. C. P.; Jovall, P. A.; Mantsch, H. H.; Siminovitch, D. J. *J. Chem. Phys.* **1987**, *88*, 1260−1263.
(161) Siminovitch, D. J.; Ruocco, M. J.; Olejniczak, E. T.; Gupta, S. K. D.; Griffin, R. G. *Biophys. J.* **1988**, *54*, 373−381.
(162) Williams, J. C.; McDermott, A. E. *J. Phys. Chem.*, accepted for publication.
(163) Usha, M. G.; Peticolas, W. L.; Wittebort, R. J. *Biochemistry* **1991**, *30*, 3955−3962.
(164) Tse, T. Y. Thesis, College of William and Mary, 1994.
(165) Kaplan, J. I.; Garroway, A. N. *J. Magn. Reson.* **1982**, *49*, 464−475.
(166) Brandes, R.; Vold, R. R.; Vold, R. L.; Kearns, D. R. *Biochemistry* **1986**, *25*, 7744−7751.
(167) Brandes, R.; Vold, R. R.; Kearns, D. R.; Rupprecht, A. *Biochemistry* **1990**, *29*, 1717−1721.
(168) Kintanar, A.; Huang, W.-C.; Schindele, D. C.; Wemmer, D. E.; Drobny, G. *Biochemistry* **1989**, *28*, 282−293.
(169) Alam, T. M.; Orban, J.; Drobny, G. *Biochemistry* **1990**, *29*, 9610−9617.
(170) Mattiello, D. L. Thesis, University of Washington, 1993.
(171) Copié, V.; McDermott, A. E.; Beshah, K.; Williams, J. C.; Spijker-Assink, M.; Gebhard, R.; Lugtenburg, J.; Herzfeld, J.; Griffin, R. G. *Biochemistry* **1994**, *33*, 3280−3286.
(172) Kinsey, R. A.; Kintanar, A.; Tsai, M.-D.; Smith, R. L.; Janes, N.; Oldfield, E. *J. Biol. Chem.* **1981**, *256*, 4146−4149.
(173) Prosser, R. S.; Davis, J. H.; Dahlquist, F. W.; Lindorfer, M. A. *Biochemistry* **1991**, *30*, 4687−4696.
(174) Lazo, N. D.; Hu, W.; Cross, T. A. *J. Magn. Reson., Ser. B* **1995**, *107*, 43−50.
(175) Bowers, J. L.; Oldfield, E. *Biochemistry* **1988**, *27*, 5156−5161.
(176) Tuzi, S.; Naito, A.; Saito, H. *Eur. J. Biochem.* **1993**, *218*, 837−844.
(177) Keniry, M. A.; Rothgeb, T. M.; Smith, R. L.; Gutowsky, H. S.; Oldfield, E. *Biochemistry* **1983**, *22*, 1917−1926.
(178) Gall, C. M.; Cross, T. A.; DiVerdi, J. A.; Opella, S. J. *Proc. Natl. Acad. Sci. U.S.A.* **1982**, *79*, 101−105.
(179) Williams, J. C., and McDermott, A. E. *Biochemistry* **1995**, *34*, 8309−8319.
(180) Zhang, H.; Bryant, R. G. *Biophys. J.* **1995**, *68*, 303−311.
(181) Mack, J. W.; Torchia, D. A.; Steinert, P. M. *Biochemistry* **1988**, *27*, 5418−5426.
(182) Jelinski, L. W.; Torchia, D. A. *J. Mol. Biol.* **1980**, *138*, 255−272. Sarkar, S. K.; Sullivan, C. E.; Torchia, D. A. *Biochemistry* **1985**, *24*, 2348−2354.
(183) Sarkar, S. K.; Hiyama, Y.; Niu, C. H.; Young, P. E.; Gerig, J. T.; Torchia, D. A. *Biochemistry* **1987**, *26*, 6793−6800.
(184) Kristensen, J. H.; Bildsoe, H.; Jacobsen, H. J.; Nielsen, N. C. *J. Magn. Reson.* **1992**, *100*, 437−443.
(185) Long, J. R.; Sun, B. Q.; A. Bowen; Griffin, R. G. *J. Am. Chem. Soc.* **1994**, *116*, 11950−11956.
(186) Cole, H. B. R.; Sparks, S. W.; Torchia, D. A. *Proc. Natl. Acad. Sci. U.S.A.* **1988**, *85*, 6362−6365.
(187) Lolis, E.; Alber, T.; Davenport, R. C.; Rose, D.; Hartman, F. C.; Petsko, G. A. *Biochemistry* **1990**, *29*, 6609−6618.
(188) Lolis, E.; Petsko, G. A. *Biochemistry* **1990**, *29*, 6619−6625.

JP9606117